Cell Reports

Article

Molecular archaeology of human cognitive traits

Graphical abstract

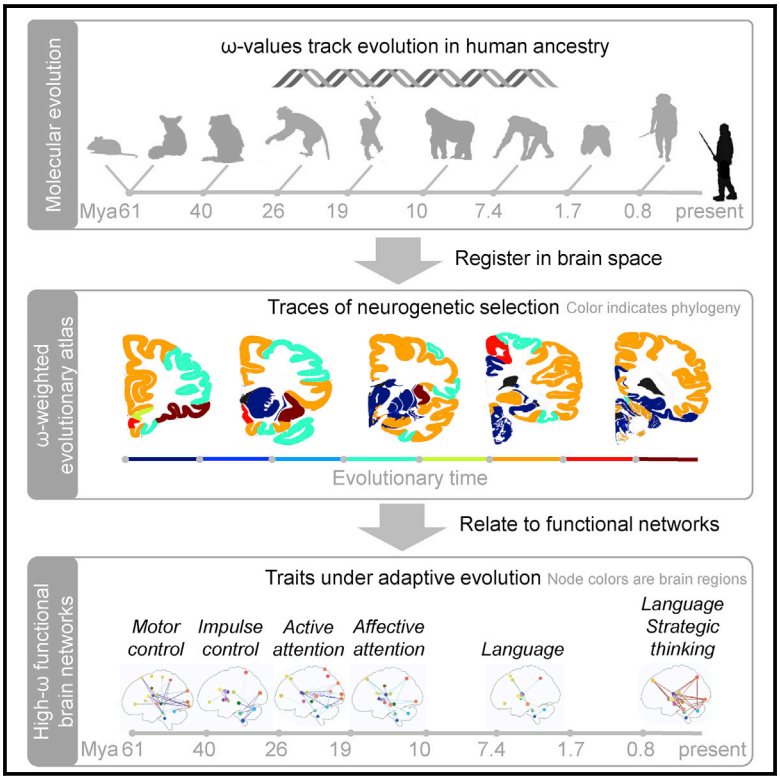

Highlights

- Projecting selection markers onto human brain space generated by evolutionary brain atlas
- Evolution shifts from motor tasks in anthropoids to attention in hominoid ancestors
- Earliest signatures of language in a hominin ancestor 7.4–1.7 mya
- Co-evolution of language and strategic thinking in the lineage to modern humans

Authors

Joanna Kaczanowska, Florian Ganglberger, Olga Chernomor, ..., Arndt von Haeseler, Katja Bühler, Wulf Haubensak

Correspondence

wulf.haubensak@meduniwien.ac.at

In brief

Kaczanowska et al. reconstruct multigenic selection in the human brain, retracing adaptive evolution from motor control in anthropoid ancestry to emerging language skills in early hominins. Anatomically modern humans separated from archaic hominins by further co-evolving language alongside strategic thinking. These traces reflect increasingly complex cognitive demands in archaic environments.

Kaczanowska et al., 2022, Cell Reports *40*, 111287
August 30, 2022
https://doi.org/10.1016/j.celrep.2022.111287

CellPress

Cell Reports

CellPress
OPEN ACCESS

Article

Molecular archaeology of human cognitive traits

Joanna Kaczanowska,[1,9] Florian Ganglberger,[2,9] Olga Chernomor,[3,9] Dominic Kargl,[1,8] Bence Galik,[4] Andreas Hess,[5] Yoshan Moodley,[6] Arndt von Haeseler,[3,7] Katja Bühler,[2] and Wulf Haubensak[1,8,10,*]

[1]Research Institute of Molecular Pathology (IMP), Vienna Biocenter (VBC), Campus-Vienna-Biocenter 1, 1030 Vienna, Austria
[2]VRVis Research Center, Donau-City Strasse 11, 1220 Vienna, Austria
[3]Center for Integrative Bioinformatics Vienna (CIBIV), Max Perutz Labs, University of Vienna, Medical University of Vienna, Dr. Bohr Gasse 9, 1030 Vienna, Austria
[4]Bioinformatics and Scientific Computing, Vienna Biocenter Core Facilities (VBCF), Dr. Bohr Gasse 3, 1030 Vienna, Austria
[5]Institute of Experimental and Clinical Pharmacology and Toxicology, Friedrich-Alexander University Erlangen-Nuremberg, Fahrstrasse 17, 91054 Erlangen, Germany
[6]Department of Zoology, University of Venda, Private Bag X5050, Thohoyandou, Republic of South Africa
[7]Faculty of Computer Science, University of Vienna, Währinger Str. 29, 1090 Vienna, Austria
[8]Department of Neuronal Cell Biology, Center for Brain Research, Medical University of Vienna, Vienna, Austria
[9]These authors contributed equally
[10]Lead contact
*Correspondence: wulf.haubensak@meduniwien.ac.at
https://doi.org/10.1016/j.celrep.2022.111287

SUMMARY

The brains and minds of our human ancestors remain inaccessible for experimental exploration. Therefore, we reconstructed human cognitive evolution by projecting nonsynonymous/synonymous rate ratios (ω values) in mammalian phylogeny onto the anatomically modern human (AMH) brain. This atlas retraces human neurogenetic selection and allows imputation of ancestral evolution in task-related functional networks (FNs). Adaptive evolution (high ω values) is associated with excitatory neurons and synaptic function. It shifted from FNs for motor control in anthropoid ancestry (60–41 mya) to attention in ancient hominoids (26–19 mya) and hominids (19–7.4 mya). Selection in FNs for language emerged with an early hominin ancestor (7.4–1.7 mya) and was later accompanied by adaptive evolution in FNs for strategic thinking during recent (0.8 mya–present) speciation of AMHs. This pattern mirrors increasingly complex cognitive demands and suggests that co-selection for language alongside strategic thinking may have separated AMHs from their archaic Denisovan and Neanderthal relatives.

INTRODUCTION

There is a genuine interest in exploring the emergence of human cognitive traits from our primate and hominin ancestors. Humans have evolved a unique set of advanced cognitive functions related to emotionality, sociality, abstraction, and language. While these functions are also present in primates, they are not as developed (Lieberman, 2016; MacLean, 2016; Parr et al., 2005; Roth and Dicke, 2005). To date, our understanding of the anatomically modern human (AMH) cognitive past primarily came from archaeological records and indicated particular dynamics in social group size, cooperative behavior, tool use, and altruism in early *Homo sapiens* (Hill et al., 2009). Comparatively, archeological artifacts and the fossil record of Neanderthals, one of our closest relatives, do not show the same degree of cognitive flexibility or symbolic activities (Marean, 2015). To reconstruct the evolutionary history of cognitive traits more comprehensively, we must travel back further into our distal ancestral lineage, where archaeological records become scarce.

To fill this gap in our archaeological history, comparative functional neuroanatomy retraced cognitive evolution based on incremental neuroanatomical changes along the mammalian lineage (Bauernfeind et al., 2015; He et al., 2017; Herculano-Houzel, 2012; MacLean, 2016; Sherwood et al., 2008; Sousa et al., 2017). This provided insights into the evolution of the size, shape (Navarrete et al., 2011; Du et al., 2018; González-Forero and Gardner, 2018; Hofman, 2014; Neubauer et al., 2018), and function (Leah, 2009; Roth, 2015) of the AMH brain. Quantitative neuroanatomical measures, such as increases in regional volumes, gene-expression boundaries, or cell (type) numbers, serve as proxies to infer evolutionary selection (Table S1). These changes in structural organization and connectivity point to complex patterns in neurocognitive evolution (Balezeau et al., 2020; Mantini et al., 2013). However, albeit extremely informative, most comparative anatomical approaches are limited to extrapolating ancestral states from experimentally accessible species that can be mapped with high anatomical resolution. This is particularly difficult for tracing evolutionary history throughout periods where only endocasts of skulls remain (e.g., Neanderthals), thereby limiting insights to inferences from the brain surface.

Evolutionary genetics, on the other hand, allows us to analyze archaic material and infer ancestral differences in cognitive traits from genetic mutations (Pääbo, 2014). This can identify and

hallmark events in AMH brain evolution (Enard et al., 2002; Florio et al., 2015; Nuttle et al., 2016). However, the underlying mutations are typically interpreted in isolation, making it difficult to capture potentially synergistic effects of multigenic co-evolution distributed across functionally coupled brain-wide networks. Indeed, the evolution of complex cognitive traits, particularly language, are thought to be dominated by the compound effect of many genes (DeSalle and Tattersall, 2018) and across distributed brain networks.

Here, we build upon these foundations by fusing neuroanatomical and genetic methods to benefit from the strengths of each approach. Genetic analysis allows the extrapolation of ancestral states, while neuroanatomy provides network context for identifying multigenic effects. By retracing our cognitive past, we are ultimately interested in identifying traits under evolutionary selection, that is, those that have resulted in adaptive phenotypes. Evolutionary pressures leave robust, distinct signatures that are measurable within the genome (Miyata and Yasunaga, 1980; Nei and Gojobori, 1986). Genetic information contains genome-wide (preserved) signatures of evolutionary adaptations that can be mapped along phylogenies (including ancestral lines), even where the species themselves are extinct.

Highly parallel sequencing techniques have generated whole genomes of both extant (Zerbino et al., 2018) and extinct species (Green et al., 2010; Meyer et al., 2012; Prüfer et al., 2014), which can resolve the evolutionary relationships between AMHs and their recent relatives. Additionally, gene expression correlates with the mesoscale functional organization of brain networks (Richiardi et al., 2015; Ganglberger et al., 2018), in which mRNA of genes associated with a specific cognitive function accumulates in the specific brain networks supporting that function. Therefore, using genetic (Hawrylycz et al., 2012), connectomic (Ding et al., 2016), and behavioral or psychiatric (Van Essen et al., 2013) brain-data initiatives, we can attribute these genetic features directly to functional brain networks and behavioral traits (Ganglberger et al., 2018; Hawrylycz et al., 2015; Richiardi et al., 2015; Wang et al., 2015).

In this study, we reasoned that these approaches may be adapted to project evolutionary genetic attributes onto brain functional networks. We combined the strengths of evolutionary genetics and computational neuroanatomy into a brain-wide evolutionary atlas. This allows us to retrace evolutionary selection within the framework of the human brain to reconstruct cognitive evolution in AMH ancestry for which skulls and brains remain out of reach.

RESULTS

Reconstructing traces of evolutionary selection in AMH phylogeny

Evolutionary forces favor various types of genetic changes. In addition to protein-coding mutations, changes to noncoding mRNA, regulatory sequences, insertions or deletions (indels), species-specific genes/duplications, and copy-number variations contribute to functional adaptations (Halligan et al., 2013) but underlie the same macroscopic selective forces at the organismic level (Haygood et al., 2007; Fu and Akey, 2013; Doan et al., 2016). Therefore, mutations in homologous brain-expressed protein-coding genes may serve as a robust proxy to model overall organismic adaptive evolution of cognitive function in the AMH brain (Ganglberger et al., 2018; Richiardi et al., 2015).

To derive the evolutionary history of protein-coding brain-expressed genes, we collected corresponding one-to-one orthologs for 9,497 genes among major mammalian species that comprise the ancestral lineage leading to AMHs, namely mouse (rodents), bush baby (prosimians), marmoset (New World monkeys), macaque (Old World monkeys), gibbon (lesser apes), gorilla and chimpanzee (great apes), extinct hominins Denisovan and Neanderthal, and AMH (see STAR Methods, data collection). For each gene, we deduced its gene tree using maximum likelihood estimation (see STAR Methods, phylogenetic analysis). Gene trees may differ from species trees due to incomplete lineage sorting (ILS), which is particularly strong among recently and quickly diverged species (Avise et al., 1983; Pamilo and Nei, 1988). Evolutionary relationships among nonhominid species on most gene trees agreed with the accepted species tree (see STAR Methods, phylogenetic analysis, and Figure S12). However, ILS was severe within the gorilla-chimpanzee-AMH triplet (Ebersberger et al., 2007) and the Denisovan-Neanderthal-AMH triplet (Meyer et al., 2014; Reich et al., 2010), resulting in nine alternative gene trees, hereafter referred to as ILS trees. The most frequently inferred gene tree (referred to as tree 1; see Figure 1A) aligns with the commonly accepted species relationship between gorilla, chimpanzee, and AMH and supports the mitochondrial (mt)DNA relationship between archaic and modern humans (Meyer et al., 2014). To control for ILS among our sample of gene trees, we focused on genes that follow one of the nine ILS trees, reflecting the major paths of genetic evolution leading to humans. This allowed for a less biased estimation of evolutionary parameters rather than estimating from the species tree alone.

We estimated the ratios of nonsynonymous to synonymous nucleotide substitutions (ω or dN/dS) using the branch "free-rate" model for all branches in all gene trees (Yang, 1998; Yang and Nielsen, 1998) (see STAR Methods, ω calculation, and Table S2). ω measures the selection pressure (and its changes) on genes over the course of evolutionary history and is sensitive to underlying evolutionary adaptation (Boddy et al., 2017; Wang et al., 2013). Unlike other means of detecting selection (McDonald and Kreitman, 1991; Sabeti et al., 2002; Tang et al., 2007; Zhong et al., 2010), ω does not require population data (e.g., polymorphism, effective population size), which are largely unavailable for extinct species. This approach has been widely used to elucidate genomic diversification among primates (Duret and Mouchiroud, 2000; Gibbs et al., 2007; Van Der Lee et al., 2017; Marinić and Lynch, 2020; Miyata et al., 1994) as well as in the context of brain evolution (Dorus et al., 2004; Tuller et al., 2008).

Unreliable ω estimates, owing to little or no sequence divergence and/or short sequence length, were excluded from further analysis to diminish potential computational artifacts (Kryazhimskiy and Plotkin, 2008) (see STAR Methods, ω calculation, and Table S2). As expected, most excluded estimates occurred among the closely related hominids (Figure S14; Table S10). For each branch in the nine ILS trees, at least 93% of genes

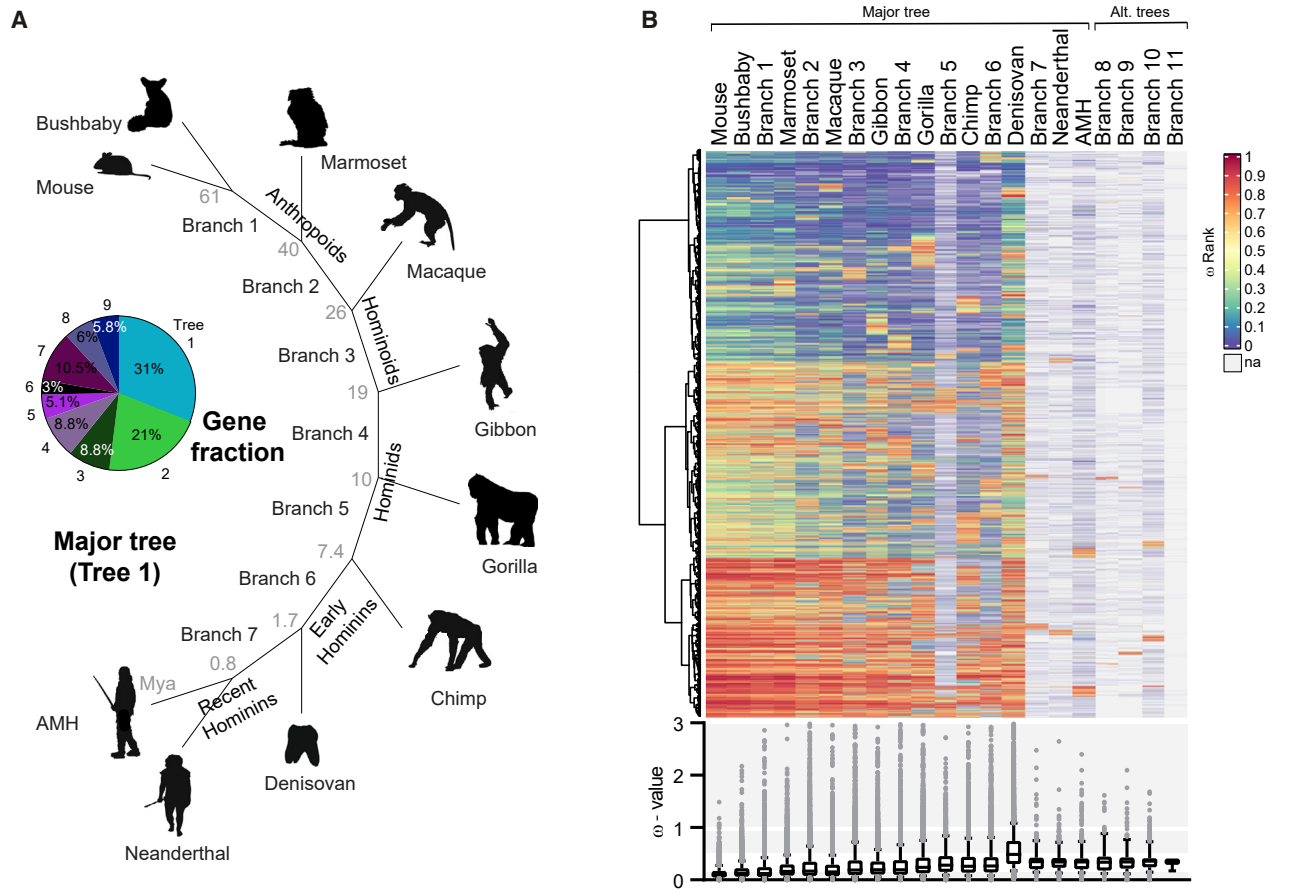

Figure 1. Reconstructing genomic selection in the AMH lineage

(A) The major (most frequently occurring) phylogenetic gene-tree topology (tree 1) of key mammalian species in the ancestral lineage leading to humans, including extinct hominins (Denisovan and Neanderthal). Inset shows the proportion of genes matching the nine alternative ILS gene-tree topologies (Figure S1). Approximate phylogenetic times from mtDNA (Figure S15).

(B) Hierarchical clustering of ω values of 8,978 AMH brain genes in the ancestral mammalian phylogeny (tree 1) and alternative hominid branches (8–11) in ILS topologies. Top, after filtering, the ω values were rank normalized in columns for each branch. Color codes indicate normalized rank. The alternative hominid branches (8–11) are visualized in Figure S1, and the sparsity of ranked genes in these cases emerged from less frequent tree topologies (fewer genes were available). Genetically proximal species (e.g., Neanderthal, AMH) naturally resulted in fewer genes with available ω values between these species and fewer genes (i.e., fewer substitutions) with reliable ω estimates Note that these lower gene branches (columns 8, 9, and 11) and phylogenies (Figure S1) were below the significance cutoff in the atlas (Figure S2; Data S2) and network biclustering. Bottom, the distribution of absolute ω values at individual branches. Shaded areas indicate purifying selection (ω = 0) versus close to neutral (ω = 0.5–1) and positive selection (ω > 1). Boxplots depict the median with 0.25 and 0.75 percentiles and whiskers at 0.1 and 0.9 percentiles.

were under purifying selection, corroborating previous findings (Gibbs et al., 2007; Mikkelsen et al., 2005), except for the Denisovan branch, where only 87% of genes were ω <1.

Then, we rank normalized ω values for each branch (considering all gene trees; see STAR Methods, genetic data preparation, and Table S3) to further reduce the influence of outliers that had not yet been filtered out. These ranked data revealed distinct clusters of co-evolving genes, which shared similar evolutionary patterns of high- and low-ranked ω (Figure 1B). The underlying absolute ω values (Figure 1B, bottom panel) reflect adaptive evolution by close to neutral (ω = 0.5–1) and positive selection (ω > 1) as well as strong purifying selection (ω = 0) across the ancestral evolution of the AMH brain. The overall median increase in ω among protein coding suggests that brain-expressed genes (whose ω could be reliably estimated) may have been under less purifying selection in hominids (i.e., branch 4 and later).

An evolutionary atlas of neurogenetic selection in the human lineage

In the brain, evolutionary forces associated with a given gene typically function through its neuroanatomical gene-expression profile (i.e., the sites where the gene is expressed). Therefore, we used the local aggregate of evolutionary attributes (e.g., ω values) of all the genes expressed at a given site to estimate the overall selection acting on this brain region.

We weighted the high-resolution local gene-expression data of 3,702 biopsy sites in the AMH reference brain (Ding et al.,

2016; Hawrylycz et al., 2012) with branch-wise, rank-ordered ω values (Tables S2 and S3; see STAR Methods, generating ω-weighted maps). The biopsy-site-level information reflects the aggregated ranked ω-weighted gene expression (i.e., each gene's expression value multiplied by its ranked ω, averaged over all genes) for all branches, including alternative hominid branches (8–11 in ILS trees; Figure 1B) in the ancestral phylogeny.

For structural-functional assessment, we down-sampled this high-resolution data to regional level maps (see Data S2 for brain-wide maps, anatomically annotated as present in https://human.brain-map.org/; see Figure S2A for representative sections). For statistical evaluation, aggregate values were compared with aggregate products in which ranked ω values were shuffled (see STAR Methods, generating ω-weighted maps). These data reveal hotspots with higher-than-expected ω ranks, under neutral or positive selection (as opposed to low ω ranks indicating strong purifying selection). Such neutral or positive selection in part reflects relaxation from strong purifying selection and can drive variation in phenotypic differentiation leading to evolutionary innovations (Hunt et al., 2011; Ohno, 1970; Lahti et al., 2009; Lynch and Conery, 2000; Snell-Rood et al., 2010) and speciation (Templeton, 2008). To illustrate the emerging phylogenetic pattern, we combined these data into maps of highly ranked ω (see STAR Methods, generating ω-weighted maps) along the most frequent gene-tree topology (tree 1; Figure 1A). This generated lineage-wide maps of neurogenetic selection in the AMH brain (Table S4 and Data S2 for a brain-wide maps). We note that these maps are entirely genetically driven and are independent of homology among brain areas of different species. Therefore, they reflect traces of major adaptive selection (neutral or positive selection in part reflecting a relaxation of constraints) through the evolutionary history of successive ancestral mammalian divergences, mapped directly onto the AMH brain. Although the full dataset (Table S2; Data S2) can serve as a resource for further in-depth exploration, here we inspected the consequent maps of representative sections (Figure S2) for a broad neuroanatomical interpretation.

Overall, the evolutionary maps (Figure S2A) reveal a complex pattern of selection across many subcortical (e.g., branches 1–3: midbrain, hypothalamus, basal forebrain) and cortical (e.g., branch 6–AMH: occipital-temporal gyrus, somatosensory association cortex, superior frontal gyrus) regions. To visualize the temporal distribution more directly, individual maps (Figure S2A) were combined into a 3,702 biopsy-site-level temporo-spatial atlas, where each brain region is color coded by the branch with the smallest p value (ω peak) (see Figure 2 for representative sections and Data S3 for a brain-wide atlas). Ranked ω peaks from early primate ancestors (Figure 2; branch 1; medulla, hippocampal formation, and claustrum) may reflect the evolution of basic cognitive traits, such as autonomic regulation, spatial memory, attention, and consciousness (claustrum; Smith et al., 2019; Crick and Koch, 2003; see Table S11). In contrast, ranked ω peaks from hominin branches expanded to higher, cortical areas (branches 6, 7, and AMH; Figure 2). These later traces in prefrontal and temporal cortical areas may reflect higher cognitive evolution (Mattson, 2014). For instance, the superior temporal gyrus (STG), which includes Wernicke's area involved in language perception, and the inferior frontal gyrus (IFG) opercularis and triangular subdivisions, which largely overlap with Broca's area and are linked to speech production, both accumulated significant ω weight in branch 6 (Figure S2; Data S2), with a temporal trend from language understanding in branch 6 (STG; Figure 2; Data S3) to language production (triangular part of IFG [trIFG]; Figure 2; Data S3). Collectively, this atlas provides a resource for mining traces of ancestral neurogenetic evolution in the AMH brain, complementing comparative neuroanatomical data and previous inferences about cognitive evolution in our archaic ancestry (Table S1).

Co-evolution networks in the AMH brain

To visualize patterns of co-evolving brain regions contained within the temporo-spatial atlas (Data S3; Figure 2), we hierarchically clustered (Ward's D2 criterion) brain areas by their correlation of mean-ranked, ω-weighted gene-expression p values (Data S2; Figure S2). This yielded eight clusters (additional clusters did not reveal higher variance), which delineated brain-wide co-evolution networks with a similar history of selection (see Figure 3A for representative sections and Data S4 for brain-wide maps).

Plotting the mean-ranked, ω-weighted gene-expression p values for each branch against its evolutionary divergence time (see STAR Methods, phylogenetic timeline) corroborated the pattern observed in the visual interpretation (results, an evolutionary atlas of neurogenetic selection in the human lineage). High ω ranks shifted from subcortical regions in earlier primate ancestry to increasingly more cortical regions at later time points during hominid and hominin evolution (Figure 3B, bottom; subcortical [clusters 1 and 3] and cortical [clusters 5 and 6] averages). These data yielded notable subpatterns. Clusters 1 and 3 decreased from approximately 19 mya to the present, indicating a shift toward purifying selection in the more "ancient" brain regions (e.g., pons, medulla, thalamus, hypothalamus, and midbrain), which became fixed with the divergence of greater apes from lesser apes (Figure 3B; branch 4). In contrast, a subset of cortical (dorsomedial prefrontal cortex in cognitive processing) and limbic structures (amygdala involved in affective processing; cluster 4) followed the inverse pattern, indicating functional rearrangements with the emergence of hominids, particularly among hominins (Figure 3B) in cingulate (cluster 7) and temporal cortices (cluster 8). The high-ranked ω of mixed clusters (clusters 2 and 4 and their average; see Figure 2B) suggests that evolutionarily, most flexible adaptations engage networks that span brain hierarchies.

Ancient traces from motor control to language and strategic thinking in the AMH brain

Building upon these temporo-spatial dynamics, we explored cognitive functions embedded in co-evolution networks (Figure S3) explicitly by fusing the spatially registered temporal evolutionary genetic data contained within our atlas directly with spatially registered functional networks (FNs) in the AMH brain. To this end, a total of 22 FNs were assembled from task-evoked functional magnetic resonance imaging (MRI) from the Human Connectome Project (HCP; 11 FNs, Figure S4; Table S12; Van Essen et al., 2013) and functional

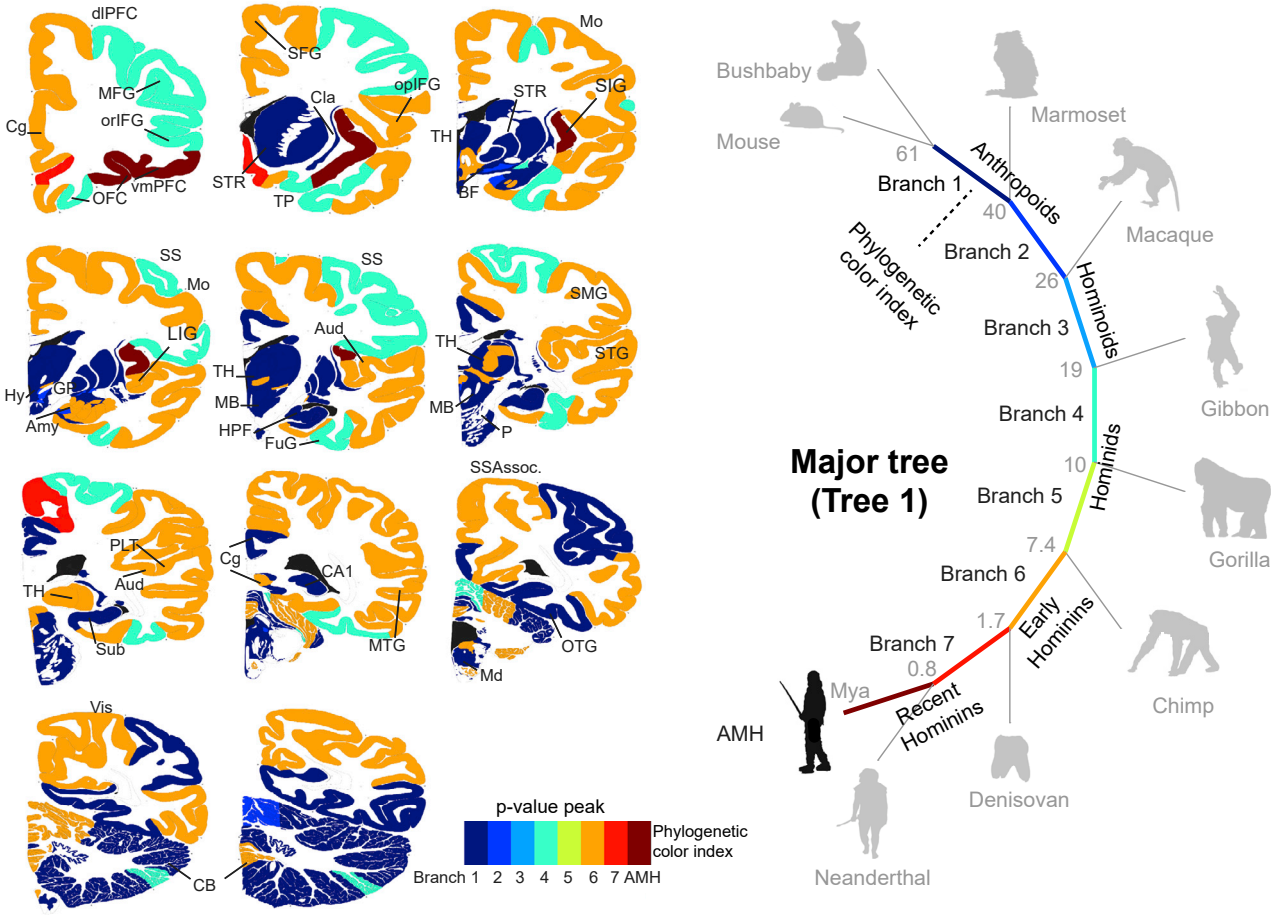

Figure 2. Evolutionary traces of genetic selection in the AMH brain

Peak ω weighted temporo-spatial atlas of the cumulative load of rank-normalized ω-weighted gene expression on the most frequent gene tree (tree 1; Figure 1A), projected onto coronal cross-sections of the AMH brain (left). Colors indicate the branches (right) with the absolute peak in rank-normalized ω-weighted cumulative gene expression in each brain region (Figure S2). Note that the atlas was originally computed for 3,702 biopsy sites (Table S4; Data S3) but is visualized here on a subset of 11 representative slices at a regional level for readability.

neuroanatomical literature (11 FNs; Figure S4; Table S13). These 22 FNs were selected *a priori* to cover the human-relevant cognitive spectrum across emotionality, sociality, abstraction, and language. This enabled temporo-spatial pattern mining by generalized biclustering (Curry, 2014) for FNs co-evolving with highly ranked ω gene sets (i.e., FNs with traces of positive or neutral [versus purifying] selection; see Figure 4A). Specifically, we biclustered 8,974 brain genes based on their ranked ω and their 3,702 site-level resolution gene-expression correlation to FNs (STAR Methods, subspace pattern mining for network evolution via biclustering; Table S7). Custom criteria were fitted to identify the most diverse biclusters of co-evolving genes ($\geq$0.90 ranked ω for the given branches) with high specificity for FNs (high spatial correlation for the same networks from Tables S12 and S6).

We applied this workflow to the collective gene-tree topologies spanning 61 my of neurocognitive evolution from prosimians to hominin ancestry (branches 1–11 and AMH) (Figures 1A and S1; STAR Methods, phylogenetic analysis), yielding statistically stable biclusters (Table S5) for distinct branches. These clusters retrace signatures of adaptive selection (i.e., high ω) in FNs of the AMH brain, highlighting cognitive traits under the most prominent evolution along AMH ancestry. Notably, the average absolute ω of these high-ranked ω biclusters indicates that these potential neurocognitive adaptations were, at least in part, driven by positive selection (ω > 1; Figure S6).

To visualize the data, we generated a 2-dimensional (2D) evolutionary landscape of the most prominent FNs networks (Figure 4C) for each of the biclusters, along with their functional domains (Tables S12 and S13) and co-evolving genes associated with behavioral/neuronal/psychiatric symptom domains (OpenTargets database: https://platform.opentargets.org/) (Carvalho-Silva et al., 2019; Ghoussaini et al., 2021) (Figure 4D).

In biclusters appearing in the earliest branches of the human lineage (branches 1–3), the top-ranked ω values were enriched in networks for motor control (motor-feet, motor-hands FNs), working memory (working memory FN), social interaction (theory of mind FN), impulse/emotion control

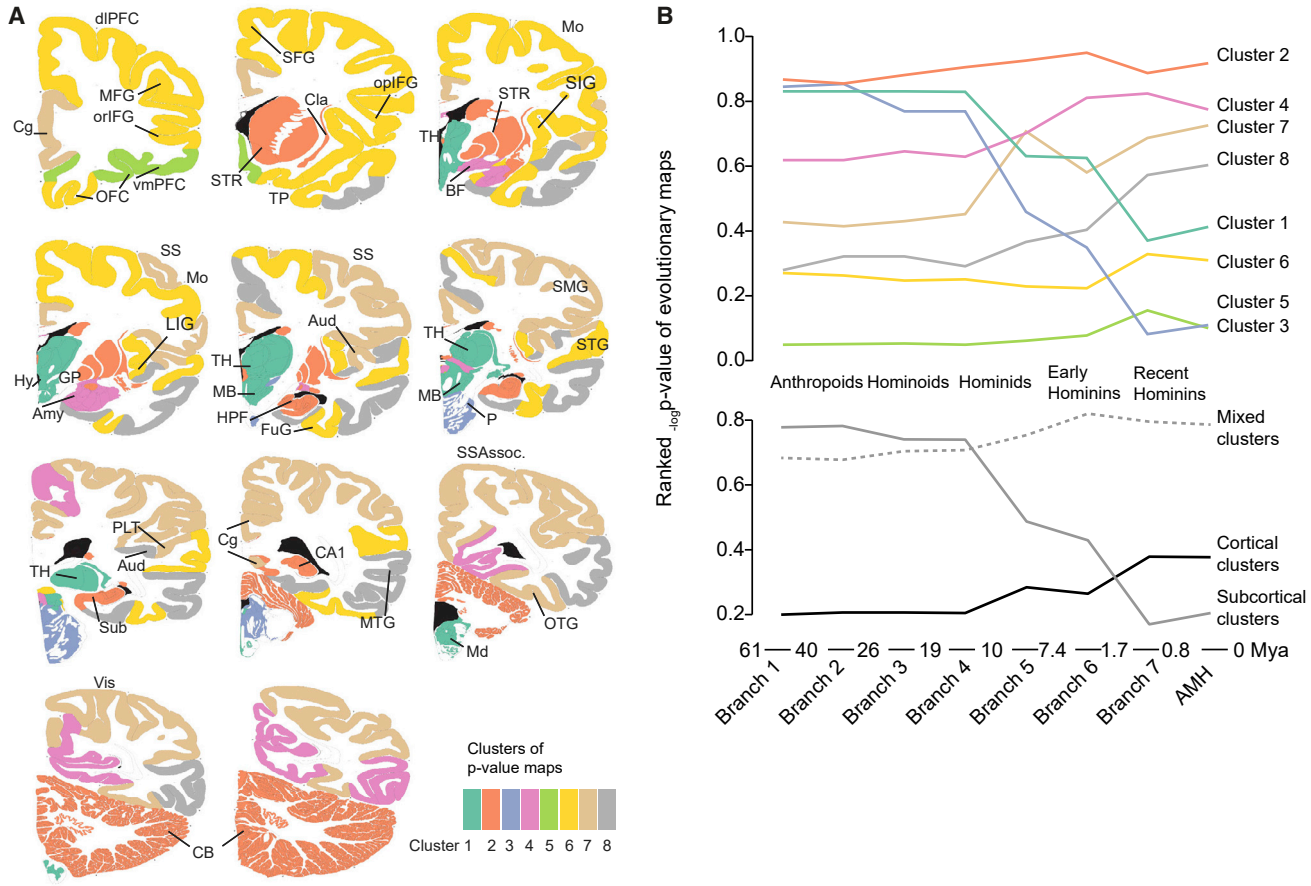

Figure 3. Co-evolution networks with shared selective history

(A) Map of human brain regions divided into eight clusters via hierarchical clustering using their mean p values (obtained from the evolutionary maps in Figure S2), representing ranked ω-weighted gene expression in brain space. Note that the atlas was originally computed for 3,702 biopsy sites (Table S4; Data S3) but is visualized on a subset of 11 representative slices at a regional level for readability.

(B) Plotting each cluster's average ranked $-\log_{10}$ p values (of the evolutionary maps in Figure S2) over the evolutionary time from branch 1 to AMH. High values close to 1 indicate high significance (i.e., higher selection pressure), whereas values closer to 0 represent low significance (i.e., lower selection pressure). Approximate phylogenetic times from mtDNA (STAR Methods, phylogenetic timeline).

(prefrontal-accumbens/prefrontal-amygdala FNs), active attention (dorsal attention FN), and action planning (fronto-parietal FN). This functional evolution is mirrored by genetic associations with the biclusters (e.g., *SNCA* with Parkinson and motor control, affective processing, *ATF4* with neuronal plasticity and behavior; Green et al., 2008) (Figure 4C; Data S1).

In branch 4, biclusters shifted toward networks for affective attention (salience FN), which are genetically associated with hypocretin neuropeptide precursor (*HCRT*) and wakefulness (Thannickal et al., 2000) (Data S1).

Interestingly, the next prominent bicluster emerged in branch 6, a key hominin ancestor that evolved prior to the divergence of AMH, Denisovan, and Neanderthal, in the central executive FN (CEN). This finding suggests evolutionary selection for cognitive processing during that period (Figures 4B and 4C). At the genetic level, the bicluster included *NCEH1*, which is linked to cholesterol metabolism and cognition (Schreurs, 2010), *IGSF11*, which is associated with intelligence (Data S1), and *FOXP2*, associated with a broad range of co-evolving higher cognitive functions (e.g., mathematical skills; Data S1; for its association with language, see below).

In contrast, branch 9, representing a gene set with a common gorilla and chimpanzee ancestry, biclustered with visuospatial processing (visuospatial FN) and was genetically associated with cholinergic receptor *CHRNA2*, a modulator of visual attention (Lawrence et al., 2002) (Data S1).

Finally, recent hominin evolution in direct AMH ancestry (i.e., branches 7 and 10) left selection traces in networks for introspection (default mode FN), emotion recognition/affective processing (emotional faces/cortico-limbic FNs), sensorimotor integration/motor control (sensorimotor/motor-hands FNs), language/abstract thinking (language/relational processing FNs), and passive attention (ventral attention FN). Genetically, this is reflected by associations with affective and higher cognitive function (*ARHGEF11*, *CHL1*, *FREM1*) (Lee et al., 2018; Mizuki et al., 2014, 2017) (Data S1).

During AMH speciation from archaic hominins (i.e., the AMH branch), highly ranked ω biclusters were linked to working

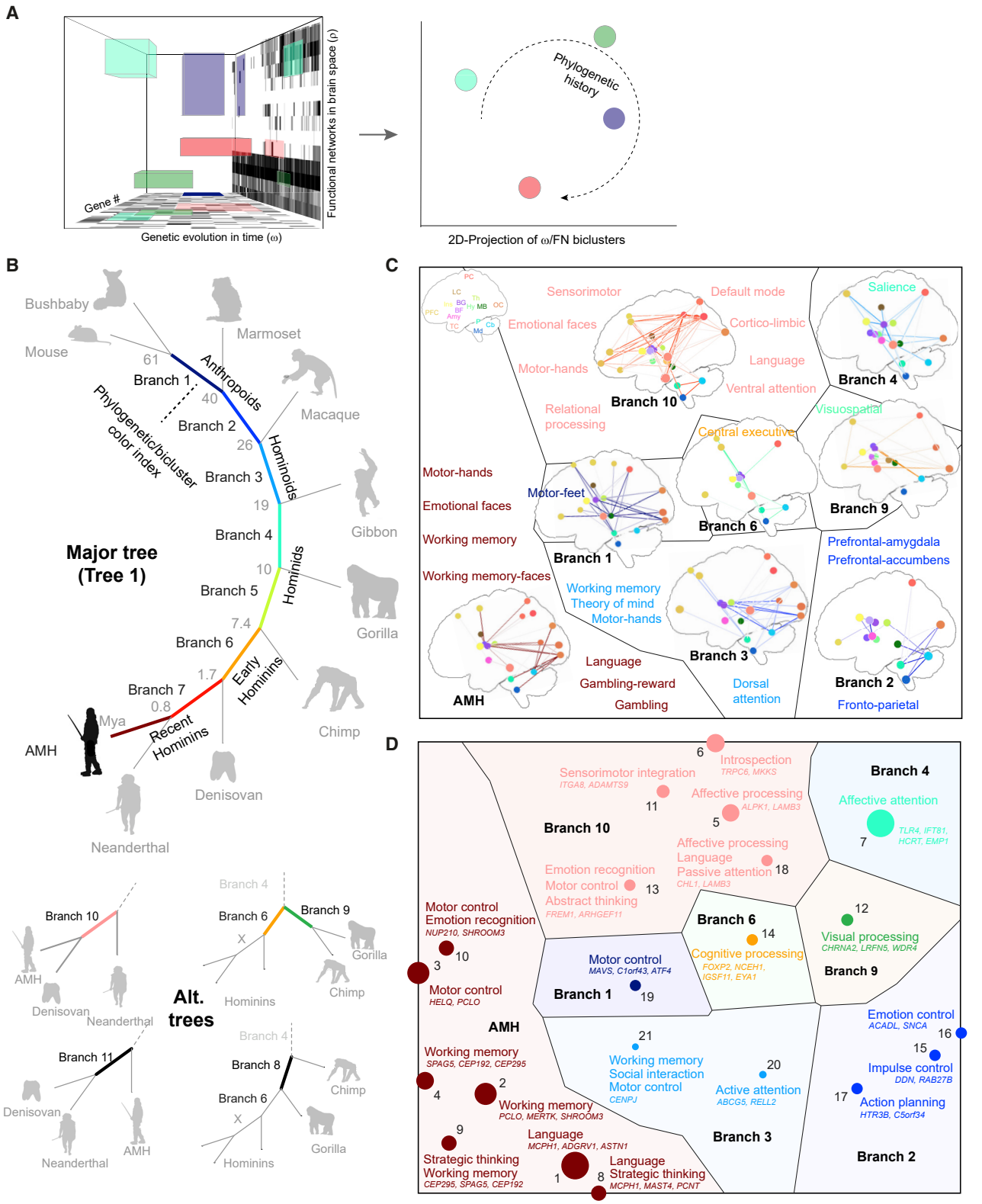

(legend on next page)

memory (working memory and working memory-face FNs), strategic thinking (gambling and gambling-reward FNs), and, most notably, language (language FN). Although these clusters partially overlap at the level of FNs (e.g., language, motor-hands, and emotional faces FNs) with branch 10, the genetic components are notably different but remain associated with higher cognitive functions. *MCPH1* controls cortex size and adult neuronal function and is under positive selection in humans (Shi et al., 2019; Jackson et al., 2002). *PCLO* is associated with synaptic function and cortical connectivity (Lee et al., 2017), and *ASTN1* is linked to mathematical and emotional abilities. *SPAG5* impacts neuronal development (Asami et al., 2011), mental abilities, and potentially language (Murphy and Benítez-Burraco, 2016) (Data S1). This shift in the genetic basis for these cognitive functions may reflect the evolution of diverging molecular mechanisms for functional tuning of language and strategic thinking in AMH (compared with branches 6 and 10).

Diverging neurocognitive evolution separates archaic and modern humans

After retracing ~61 my along the distant ancestral line to AMH (Figures 2A and 4A), we next explored proximate archaic evolution more closely: branches 5–11 and AMH, plus the speciation of our closest hominid [chimpanzee] and archaic [Denisovan, Neanderthal] relatives (Brawand et al., 2011; Khaitovich et al., 2005; Romero et al., 2012) (Figure 5A).

Indeed, in addition to AMH archaic ancestors (branches 6, 10, and AMH) discussed above, here the corresponding evolutionary maps revealed significant traces of high ω ranks also in the speciation of extinct hominin relatives (i.e., Denisovan, Neanderthal; Figure S2B; Data S2).

Based on these findings, we reiterated our biclustering workflow (Figure 4A) solely using the proximate branches (Figure 5A). As expected, within the AMH branch, the algorithm recaptured similar biclusters similar to the full lineage setting (see previous section; Figures 4B and 4C, with largely overlapping characteristic networks and gene sets).

Specifically, speciation to chimp clustered with social interaction (theory of mind FN) and was genetically associated with intelligence (*PRKAG1*) (Figures 5B and 5C). Notably, the theory of mind FN was also positively selected in branch 3 in the overall analysis (Figures 4C, 4D, and S6), reflecting overall primate social evolution (Table S1). In contrast, traces of early hominin evolution (branch 6) shift toward the CEN (Figures 4B, 4C, 5B, and 5C), which may reflect a need for attention and complex problem solving in a common hominin ancestor. Interestingly, when analyzing a more restricted set of the hominin branches alone (branches 6, 7, 10, 11, and AMH), the biggest cluster of 102 genes originated in the ancestor of all hominins (branch 6) and correlated with the language FN (language FN; Table S5; Figure S5). This language cluster contained the *FOXP2* gene, reflecting its role as the canonical language-associated gene in humans, which acquired its latest point mutation around that time (Enard et al., 2002), and *ARHGAP32*, previously discussed in human cognitive evolution (Lombard and Högberg, 2021). We believe that these data represent one of the earliest neurogenetic traces of language, which coevolved with cognitive processing (CEN) (Figures 4L, 5B, and 5C) in early hominins. Importantly, language continued to be highly selected during AMH speciation compared with that in Denisovan and Neanderthal, which both lack a language bicluster. Traces of later hominin evolution (branch 10) reveal evolutionary selection of emotion recognition (emotional face FN). The AMH branch is characterized by biclusters of working memory (working memory FN), motor control (motor-hands FN), language (language FN), and a notable emphasis on strategic thinking (gambling-reward FN). The corresponding genes (Figure 5C) largely overlap with those described previously (Figure 4B) and are linked to higher cognitive function.

Denisovan hominin speciation biclustered with networks for motor control (sensorimotor, motor-hands, and motor-feet FNs), affective attention/introspection (salience/default mode FNs), affective processing/impulse/emotion control (cortico-limbic, prefrontal-accumbens/amygdala FNs), active/passive attention (dorsal/ventral attention), and action planning (fronto-parietal FNs) networks (Figures 5B and 5C). Among the co-evolving genes was *HTR2C*, which is connected to a broad spectrum of higher cognitive function (Data S1). Overall, these data suggest broad rearrangements that continued from early (branch 6) hominin evolution. Interestingly, highly ranked ω biclusters in Neanderthal, who split from the common ancestor with AMH later than Denisovan, now correlated with both strategic thinking (gambling FN) and working memory (working memory FN) (Figures 5B and 5C). This bicluster also involves *MMP17*, a neuronal metalloproteinase associated with mathematical skills (Data S1). The evolution of strategic thinking in both Neanderthal and AMHs indicates that this is an important trait in recent hominin environments. However, AMHs evolved a stronger propensity for strategic thinking (gambling and

Figure 4. Evolutionary-functional neurogenetic clusters reconstruct traces of cognitive evolution in the AMH brain

(A) Computational strategy (schematics). Left: mining brain functional evolution by biclustering of evolutionary selection (gene-wise ω ranks for branches 1–11 and AMH) and functional networks (FNs; gene-wise network correlation in brain space). Biclusters (colored blocks) represent co-evolving FNs and gene sets organized along gross phylogenic history in 2D space (right).

(B) Biclustering of FNs (Tables S12 and S6) and highest ranked ω values (with a 0.90 rank cutoff) among major and alternative gene-tree topologies.

(C) High-ranked ω (with a 0.90 rank cutoff) biclusters were embedded into a 2D evolutionary space via t-distributed stochastic neighbor embedding (t-SNE) with the combined genetic and functional/temporal overlapped as a distance measure. Individual biclusters (1–21) with highlighted neurocognitive-associated genes (OpenTargets; Data S1) and the neurocognitive categories of the corresponding FNs (Tables S12 and S6) in evolutionary history. Circle size corresponds to cluster size.

(D) Functional annotations of the clusters in (B) and visualization of the top-ranked functional brain network, generated via BrainTrawler (Ganglberger et al., 2019) and highlighting the highest spatial gene expression correlations of highly ranked ω (0.9 percentile) corresponding to associated FNs. The nodes represent anatomical regions in the left hemisphere and are color coded according to main neuroanatomical units from ABA. The edges show gene-expression correlations of the respective networks. Note that for visibility, the data are shown on a regional level, although they are computed on a 3,702 biopsy-site level, and not all network components are shown in each case (only those with the highest correlation).

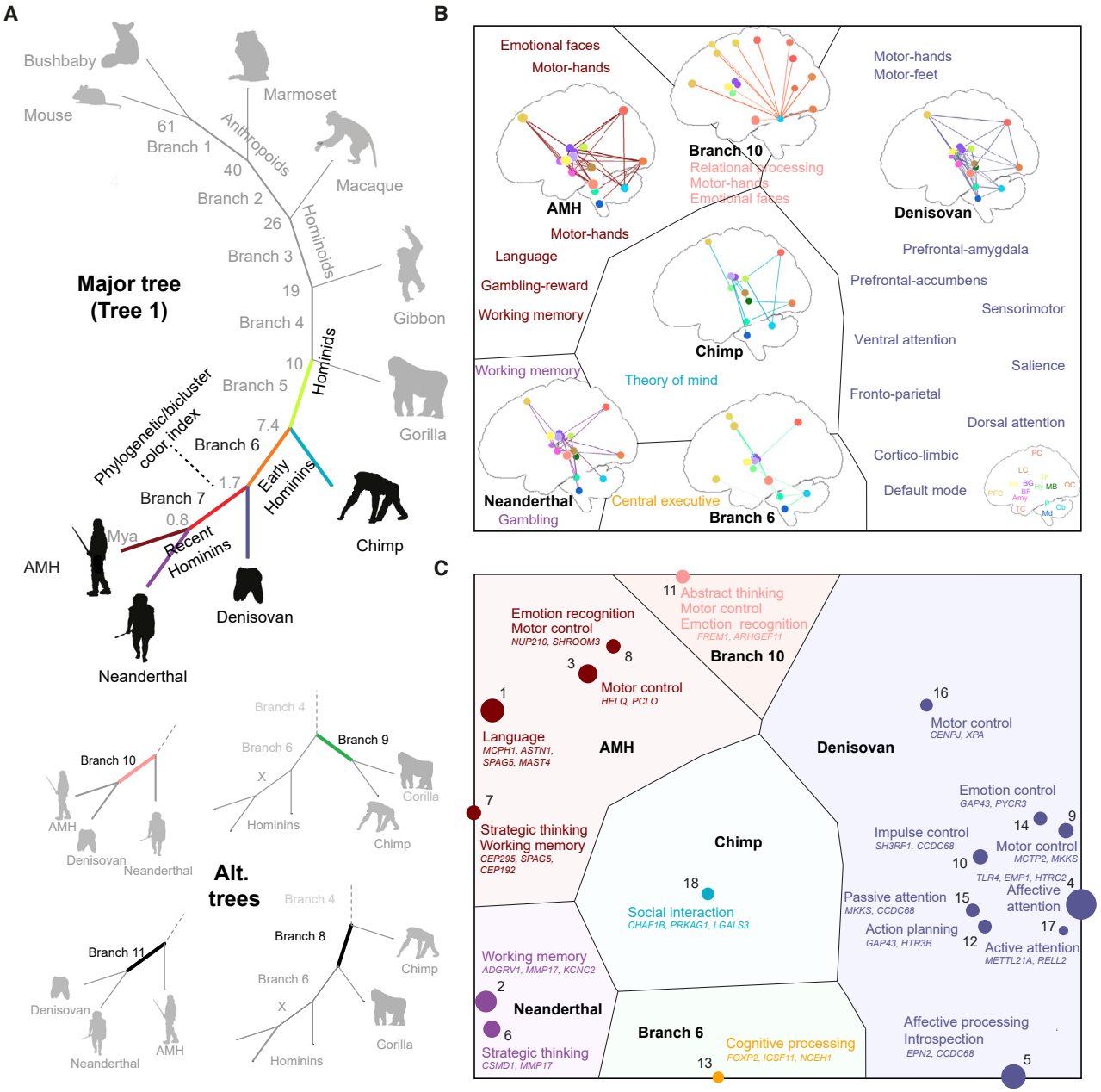

Figure 5. Imputing shared and divergent cognitive traits along AMH archaic ancestry

(A) Biclustering of FNs as in Figure 4 was performed solely on the hominid branch (branches 5–11, chimp, Denisovan, Neanderthal, and AMH).

(B) Highest-ranked ω values (at a 0.90 rank cutoff) among hominid branches (branches 5–11, chimp, Denisovan, Neanderthal, and AMH). Visualization of the top-ranked functional brain network, generated via BrainTrawler (Ganglberger et al., 2019) and highlighting the highest spatial gene-expression correlations of highly ranked ω (0.9 percentile) genes corresponding to the associated FNs. The nodes represent anatomical regions in the left hemisphere and are color coded according to the main ABA neuroanatomical structures. The edges show gene-expression correlations of the respective networks. Note that for visibility, the data are shown at a regional level, although the analysis was computed at the dense 3,702 biopsy-site level, and not all network components are shown in each case (only those with the highest correlation).

(C) High-ranked ω (at 0.90 rank cut-off) biclusters were embedded into 2D evolutionary space via t-SNE with the combined genetic and functional/temporal overlap as the distance measure. Individual biclusters (1–18) with highlighted neurocognitive associated genes (OpenTargets; Data S1) and the neurocognitive categories of the corresponding FN (Tables S12 and S6) in evolutionary history. Circle size corresponds to cluster size.

gambling-reward FNs with the highest average ω in AMHs; Figure S6). Together with the prominent traces for language, these data suggest that the co-evolution of strategic thinking and language were particularly dominant traits in the evolution of AMH.

Taken together, our approach traced evolutionary adaptions from strong purifying selection throughout ~61 my of primate evolution (Figures S6, left, bicluster averages of $\omega > 0.5$, and S11). The identified cognitive traits associated with these deviations arose from complex processes that exploited evolutionary freedoms in brain FNs, various cellular networks, diverse molecular functional interactions, and single gene effects, with hotspots at each of these levels (Figure S11).

Moreover, along mammalian phylogenies, periods of molecular and organismic divergence alternate with periods of strong purifying selection ($\omega = 0$), when functions are relatively fixed (Kosiol et al., 2008). Therefore, we contrast our findings associated with highly ranked ω to patterns of purifying selection by repeating biclustering with low ranked ω (Figure S6, right). The occurrence of the same FN (Figure S6), brain cell type (Figure S7), Ingenuity Pathway Analysis (IPA) functional category (Figure S8), or neurocognitive association (Figure S9) in both high- and low-ranked ω biclusters (but for different branches in the phylogeny) indicate shifts from purifying to relaxation of constraint and positive selection. We speculate that these cases associated with significant high- and low-ranked ω and switches between them point toward important evolutionary hotspots along the phylogeny. The occurrence of both processes in the same branch is not contradictory in this regard; rather, it may suggest high positive and purifying selection on the same FN, cell type, IPA, or genetic association, which notably emerges from a set of different genes. Overall, this can be generally reflected by the row count across both high and low ω biclusters for differing biological levels (Figures S6–S9 and S11).

DISCUSSION

This study exploited several recent big data initiatives on genomics and brain function to explore evolutionary events that shaped the brain and behavior of AMH along its ancestral lineage. Due to the absence of brain tissue specimens from ancestral hominid species, we aimed to reconstruct the ancestral evolution of cognitive functions by mining for traces of selection pressure on the AMH brain itself. We note that the extrapolation of intermediate ancestral reference brains from extant hominid and primate species can refine this approach, in principle. However, it remains unclear whether these results would be fundamentally different. Therefore, we contend that tracing these changes directly in the AMH brain is the most straightforward and informative way to study human ancestral neurocognitive evolution within the direct AMH ancestral lineage (Figure 4A) and the speciation of archaic hominins (Figure 5A).

This computational strategy explores compound neurogenetic effects on brain networks, which are untraceable when studied in isolation on a gene-by-gene basis. From the genetic perspective, the evolution of functional traits is inherently multigenic. Therefore, single-gene studies in transgenic mouse or organoid models, although mechanistically powerful (Florio et al., 2015; Di Lullo and Kriegstein, 2017; Trujillo et al., 2021), cannot easily assess genetic synergies underlying specific cognitive traits from brain-wide FNs. This study aims to complement these functional approaches by (1) holistically mapping evolutionary selection across different traits along ancestral lines and (2) identifying candidate gene sets that facilitating these adaptations. In turn, the functional exploration of our data in suitable experimental systems may reveal the underlying mechanistic detail.

We showcase an approach for reconstructing the evolutionary history of functional selection using the genetic remains of long-extinct species by projecting compound evolutionary rates of changes onto a functional anatomy reference framework. This strategy can be useful to functionally explore biological systems that are unavailable for traditional experimental studies. Our straightforward evolutionary genetic analysis could be expanded to include hominin-specific genes and population data of AMHs and archaic hominins when they become available. As it stands, the rank-order approach used in this study (Figure 1B, top) has extracted meaningful results (Figures 2, 3, 4, and 5), even within closely related species. The absolute ω estimates corresponding to these ranks (Figure 1B, bottom) allow for a secondary interpretation of these processes (Figures S6–S9): ω estimates greater than 1 indicate positive selection, low ω purifying selection, and changes from smaller to higher ω relaxation of selective constraints, which may play an important role in phenotypic differentiation (Hughes, 2012; Hunt et al., 2011; Lahti et al., 2009; Lynch and Conery, 2000; Ohno, 1970; Snell-Rood et al., 2010; Templeton, 2008). Therefore, focusing on genes with high ω should be particularly sensitive for tracing newly—at the respective time—evolving phenotypes. In line with the argument that high ω gene sets may reflect (or even drive) neurocognitive evolution, there are significant neurogenetic associations across nearly all biclusters with neuronal signaling, cognitive function, and psychiatric symptom domains (Figure S8). In most of these biclusters, we find genes under positive selection (Figure S6), indicating adaptive processes in these neurocognitive domains.

The genetic data add to the long-held notion that overall, cortical genes are more conserved than those of the subcortex (Tuller et al., 2008). In this study, we found that high ω ranks and subsequent signatures of adaptive selection are predominantly subcortical early in primate evolution while cortically accumulating within the recent human ancestry (Figure 3). These findings retraced complex mechanisms across biological levels (i.e., molecular, single-gene associations, multigenic molecular functions, cellular, and FNs) during evolutionary history. Indeed, the evolutionary dynamics within genetic, cellular, and FNs largely segregate (data not shown), suggesting complex evolutionary motifs that shape neurocognitive evolution within and between these levels of functional organization within the brain. Here, such evolutionary motifs of molecular, cellular, and network clusters become apparent. For example, key events in AMH FN evolution (Figure S11) were correlated with the dominant selection of distinct sets of mostly excitatory SFG neurons, molecular pathways related to synaptic function, and genes that are generally associated with intelligence and mathematical ability. These cross-level motifs, spanning the molecular control of synaptic function in specific sets of excitatory cells, may be

evolutionary hotspots driving computational power in the respective FNs.

In early hominoid evolution, these findings delineate a critical neurogenetic framework for archaic cognitive abilities and align with key events including the backdating of theory of mind FN (Kano et al., 2019; Krupenye et al., 2016) and ancient art (Hoffmann et al., 2018; Jaubert et al., 2016) to hominoid ancestry (Figure S6). Our computational neuroarchaeological data also suggest that archaic ancestors (branches 6 and 10) and AMH lineages evolved networks for language as the dominant trait. Interestingly, there is temporal shift in selection from Wernicke-to Broca-related areas (Figure 2; Data S3). This sequence is consistent with a long-standing hypothesis that more rudimentary vocal understanding may have evolved prior to the advanced ability for speech production (Jarvis, 2019). The selection of genes expressed in language networks had already occurred by the time archaic *Homo* species evolved. Therefore, it is plausible that evolutionary pressure for verbal communication had already evolved in *Homo erectus* in Africa (branch 6) with traces of positive selection (Figure S6) long before this species migrated to Eurasia and gave rise to Neanderthals and Denisovans. This notion places the time frame for the evolution of language prior to the earliest divergence among the studied hominid species, between approximately 6 mya to 500 kya. Further, this identifies language as a dominant multigenic trait across the neurocognitive spectrum in the evolution of *Homo erectus*. In turn, this supports broader inferences that have emerged from archaeology (Wynn, 1998) and single genes (i.e., *FOXP2*) (Enard et al., 2002) and together suggests the critical evolution of language during this period. Interestingly, in later branches, archaic hominin traces of the evolutionary selection of language skills peak during AMH speciation but not within other hominins. This pattern adds insight to the long-standing interest about the timing and origin of human language (Dediu and Levinson, 2018; Lieberman, 2015), which attribute language capabilities across archaic hominins, potentially inherited from *H. erectus*, whereas further refinement of language skills is specific to AMH. Finally, in addition to the language network in AMH ancestry (branch 6), we find traces of evolution in gambling networks as a possible emerging feature of recent hominin evolution in Neanderthals (one bicluster under relaxation of constraint), which becomes even more dominant in AMH (two biclusters under positive selection). It is tempting to speculate that these divergent neurogenetic adaptations in strategic thinking and further selection of language and verbal communication may have contributed to the separation of AMH from its closest relatives and, ultimately, its evolutionary success.

In summary, we fused multimodal publicly available data into a holistic exploration of human cognitive history from genetic traces of its past. As with any neuroarchaeological method, we only suggest probable and plausible scenarios rather than settle ultimate truths. Along these lines, our predictions can be easily extended and can improve as more ancient genomes and brain data become available. We believe that such approaches serve as a valuable complement to existing evolutionary genetics and functional genetics in humanized models (organoids, transgenic animals). Here, our workflow unraveled neurogenetic selection for complex neurocognitive traits in archaic primate brains, like emotional face recognition, motor control, and working memory, along with strategic thinking (Figures 4, 5, and S5) (Mattson, 2014).

Limitations of the study

Genetically, ω values are valid proxies for genome-wide selection under the assumption that different types of genetic changes (i.e., noncoding mRNA regulatory sequences, indels, and species-specific genes/duplications and losses) likely underlie the same macroscopic selective forces at the organismic level. However, these different changes may add additional layers of functional evolution that exceed the limit of our data, but these factors should be explored in future studies. Moreover, as there are no sufficient population data across the (extinct) species set to identify polymorphic sites, we ignored polymorphisms in our analyses. Polymorphisms may lead to smaller ω values (Kryazhimskiy and Plotkin, 2008), thereby underestimating positive selection within some genes. Consequently, although high ω ranks reliably map phenotypic adaptation within brain networks, the corresponding absolute ω value may be underestimated at times.

Neuroanatomically, the brain space in this study was based on maps with biopsy site resolution and with an *a priori* defined set of FNs. As such, future studies may use a finer resolved atlas and a wider spectrum of FNs, which would lead to more nuanced differentiation. Notably, we use adult expression data to report phenotypic selection of cognitive traits. That said, developmental programs also contribute significantly to the adaptive evolution of brain function. As some patterning (Kirsch and Chechik, 2016) and wiring (Falkner et al., 2016) programs are also functional in adults, we partially capture such developmental patterning and wiring effects indirectly (e.g., neocortical expansion; Figure S8, "brain size" functional annotation). Therefore, despite not mining developmental brain evolution *per se*, our adult dataset seems to be a reasonable approximation for dissociating the evolution of adult cognitive traits for the purposes of our study. However, it is worth applying the same workflow to developmental atlases to specifically contrast developmental and adult functional evolution.

Taken together, our study provides a current snapshot of evolutionary patterns based on the data available. By iterating these workflows with more detailed/different future genomic, proteomic, single-cell, and FN network data, we will refine the interpretations of these findings and create opportunities for further insight.

STAR★METHODS

Detailed methods are provided in the online version of this paper and include the following:

- KEY RESOURCES TABLE
- RESOURCE AVAILABILITY
  - Lead contact
  - Materials availability
  - Data and code availability

SUPPLEMENTAL INFORMATION

Supplemental information can be found online at https://doi.org/10.1016/j.celrep.2022.111287.

ACKNOWLEDGMENTS

We thank Shiva Alemzadeh and Johanna Schmidt (both VRVis Research Center) for conducting the bicluster visualization. We thank Attila Gyenesei for supervising the computation of evolutionary genetic data. We thank Nathan Lawless (Böhringer Ingelheim, Computational Biology) for providing the preprocessing for the single-cell data. We thank Life Science Editors for editing assistance. F.G. and K.B. were supported by VRVis, funded by BMVIT, BMDW, Styria, SFG, and Vienna Business Agency within the scope of the FFG COMET program (854174), the Research Institute of Molecular Pathology (IMP), Boehringer Ingelheim, and the Austrian Research Promotion Agency (FFG). W.H. was supported by the Research Institute of Molecular Pathology (IMP), Boehringer Ingelheim, the Austrian Research Promotion Agency (FFG), and a grant from the European Community's Seventh Framework Programme (FP/2007-2013)/ERC grant agreement no. 311701. O.C. and A.v.H. were supported by the Austrian Science Fund – FWF (grant number I-4686).

AUTHOR CONTRIBUTIONS

J.K. designed the study, interpreted the functional genetic analysis and computational neuroanatomy, and wrote the manuscript. F.G. designed and performed computational neuroanatomy and wrote the manuscript. O.C. collected and prepared genetic data and designed and performed evolutionary genetic analyses. D.K. interpreted functional genetic analysis and computational neuroanatomy. A.v.H. designed and supervised the evolutionary genetic analyses. B.G. performed the evolutionary genetic analysis at the exploratory stage of the project. Y.M. designed the study and performed the phylogenetic timeline analysis. A.H. designed the computational neuroanatomy. K.B. designed and supervised the computational neuroanatomy. W.H. conceived the study, designed and interpreted the computational neuroanatomy, and wrote the manuscript. All authors contributed to the writing and editing of this manuscript.

DECLARATION OF INTERESTS

The authors declare no competing interests.

Received: July 24, 2019
Revised: May 20, 2022
Accepted: August 5, 2022
Published: August 30, 2022

SUPPORTING CITATIONS

The following reference appears in the Supplemental Information: Aboitiz, 2018; Andrews-Hanna et al., 2014; Assaf et al., 2020; Barks et al., 2015; Bastir et al., 2011; Belmonte et al., 2015; Beran et al., 2016; Brosnan and De Waal, 2003; Brosnan et al., 2010; Bruner et al., 2014; Castellano et al., 2014; Conway and Christiansen, 2001; Dalley et al., 2011; De Graaf et al., 2010; Dekleva et al., 2011; Fang et al., 2012; Felleman and Van Essen, 1991; Ferri et al., 2012; Friederici, 2017; Genty et al., 2009; Grant, 2016; Hanks and Summerfield., 2017; Hecht et al., 2013; Herculano-Houzel et al., 2007; Herrmann et al., 2007; Hoffecker, 2018; Hu et al., 2019; Imura and Tomonaga, 2013; Isler et al., 2008; Johansson, 2013; Kaas, 2010; Kochiyama et al., 2018; Kumar et al., 2017; Laramée and Boire, 2015; Lin et al., 2017; Menon, 2015; O'Connell et al., 2012; Ochsner et al., 2009; Pearce et al., 2013; Price, 2000; Rilling et al., 2008; Robinson et al., 1978; Salmi et al., 2020; Seeley et al., 2007; Semendeferi and Damasio, 2000; Silcox et al., 2009; Sliwa and Freiwald, 2017; Smith et al., 2009; Tattersall, 2017; Tremblay et al., 2017; Uddin and Uddin, 2017; Ullman, 2004; Urgesi et al., 2010; Vai et al., 2015; Vossel et al., 2014; Weyrich and Morris, 2017; Whiten, 2000; Whittingstall et al., 2014; Wilson and Petkov, 2011; Wynn and Coolidge, 2004; Zanto and Gazzaley, 2013.

REFERENCES

Aboitiz, F. (2018). A brain for speech. Evolutionary continuity in primate and human auditory-vocal processing. Front. Neurosci. *12*, 174. https://doi.org/10.3389/fnins.2018.00174.

Altenhoff, A.M., Glover, N.M., Train, C.M., Kaleb, K., Warwick Vesztrocy, A., Dylus, D., De Farias, T.M., Zile, K., Stevenson, C., Long, J., et al. (2018). The OMA orthology database in 2018: retrieving evolutionary relationships among all domains of life through richer web and programmatic interfaces. Nucleic Acids Res. *46*, D477–D485. https://doi.org/10.1093/nar/gkx1019.

Andrews-Hanna, J.R., Smallwood, J., and Spreng, R.N. (2014). The default network and self-generated thought: component processes, dynamic control, and clinical relevance. Ann. N. Y. Acad. Sci. *1316*, 29–52. https://doi.org/10.1111/nyas.12360.

Asami, M., Pilz, G.A., Ninkovic, J., Godinho, L., Schroeder, T., Huttner, W.B., and Götz, M. (2011). The role of Pax6 in regulating the orientation and mode of cell division of progenitors in the mouse cerebral cortex. Development *138*, 5067–5078. https://doi.org/10.1242/dev.074591.

Assaf, Y., Bouznach, A., Zomet, O., Marom, A., and Yovel, Y. (2020). Conservation of brain connectivity and wiring across the mammalian class. Nat. Neurosci. *23*, 805–808. https://doi.org/10.1038/s41593-020-0641-7.

Avise, J.C., Shapira, J.F., Daniel, S.W., Aquadro, C.F., and Lansman, R.A. (1983). Mitochondrial DNA differentiation during the speciation process in Peromyscus. Mol. Biol. Evol. *1*, 38–56. https://doi.org/10.1093/oxfordjournals.molbev.a040301.

Balezeau, F., Wilson, B., Gallardo, G., Dick, F., Hopkins, W., Anwander, A., Friederici, A.D., Griffiths, T.D., and Petkov, C.I. (2020). Primate auditory prototype in the evolution of the arcuate fasciculus. Nat. Neurosci. *23*, 611–614. https://doi.org/10.1038/s41593-020-0623-9.

Barch, D.M., Burgess, G.C., Harms, M.P., Petersen, S.E., Schlaggar, B.L., Corbetta, M., Glasser, M.F., Curtiss, S., Dixit, S., Feldt, C., et al. (2013). Function in the human connectome: task-fMRI and individual differences in behavior. Neuroimage *80*, 169–189.

Barks, S.K., Calhoun, M.E., Hopkins, W.D., Cranfield, M.R., Mudakikwa, A., Stoinski, T.S., Patterson, F.G., Erwin, J.M., Hecht, E.E., Hof, P.R., et al. (2015). Brain organization of gorillas reflects species differences in ecology. Am. J. Phys. Anthropol. *156*, 252–262. https://doi.org/10.1002/ajpa.22646.

Bastir, M., Rosas, A., Gunz, P., Peña-Melian, A., Manzi, G., Harvati, K., Kruszynski, R., Stringer, C., and Jean Jacques, H. (2011). Evolution of the base of the brain in highly encephalized human species. Nat. Commun. *2*, 588. https://doi.org/10.1038/ncomms1593.

Bauernfeind, A.L., Soderblom, E.J., Turner, M.E., Moseley, M.A., Ely, J.J., Hof, P.R., Sherwood, C.C., Wray, G.A., and Babbitt, C.C. (2015). Evolutionary divergence of gene and protein expression in the brains of humans and chimpanzees. Genome Biol. Evol. *7*, 2276–2288. https://doi.org/10.1093/gbe/evv132.

Belmonte, J., Callaway, E.M., Caddick, S.J., Churchland, P., Feng, G., Homanics, G., Lee, K.-F., Leopold, D., Miller, C., Mitchell, J., et al. (2015). Brains, genes, and primates. Neuron *86*, 617–631. https://doi.org/10.1016/j.neuron.2015.03.021.

Beran, M.J., Menzel, C.R., Parrish, A.E., Perdue, B.M., Sayers, K., David Smith, J., and Washburn, D.A. (2016). Primate cognition: attention, episodic memory, prospective memory, self-control, and metacognition as examples of cognitive control in nonhuman primates. Wiley Interdiscip. Rev. Cogn. Sci. *7*, 294–316. https://doi.org/10.1002/wcs.1397.

Boddy, A.M., Harrison, P.W., Montgomery, S.H., Caravas, J.A., Raghanti, M.A., Phillips, K.A., Mundy, N.I., and Wildman, D.E. (2017). Evidence of a

conserved molecular response to selection for increased brain size in primates. Genome Biol. Evol. *9*, 700–713. https://doi.org/10.1093/gbe/evx028.

Brawand, D., Soumillon, M., Necsulea, A., Julien, P., Csárdi, G., Harrigan, P., Weier, M., Liechti, A., Aximu-Petri, A., Kircher, M., et al. (2011). The evolution of gene expression levels in mammalian organs. Nature *478*, 343–348. https://doi.org/10.1038/nature10532.

Brosnan, S.F., and De Waal, F.B.M. (2003). Monkeys reject unequal pay. Nature *425*, 297–299. https://doi.org/10.1038/nature01963.

Brosnan, S.F., Salwiczek, L., and Bshary, R. (2010). The interplay of cognition and cooperation. Phil. Trans. Biol. Sci. *365*, 2699–2710. https://doi.org/10.1098/rstb.2010.0154.

Bruner, E., Lozano, M., Malafouris, L., Langbroek, M., Wynn, T., Coolidge, F.L., and Martin-Loeches, M. (2014). Extended mind and visuo-spatial integration: three hands for the neandertal lineage. J. Anthropol. Sci. *92*, 273–280. https://doi.org/10.4436/JASS.92009.

Carvalho-Silva, D., Pierleoni, A., Pignatelli, M., Ong, C., Fumis, L., Karamanis, N., Carmona, M., Faulconbridge, A., Hercules, A., McAuley, E., et al. (2019). Open Targets Platform: new developments and updates two years on. Nucleic Acids Res. *47*, D1056–D1065. https://doi.org/10.1093/nar/gky1133.

Castellano, S., Parra, G., Sanchez-Quinto, F.A., Racimo, F., Kuhlwilm, M., Kircher, M., Sawyer, S., et al. (2014). Patterns of coding variation in the complete exomes of three neandertals. Proc. Natl. Acad. Sci. USA *111*, 6666–6671. https://doi.org/10.1073/pnas.1405138111.

Conway, C.M., and Christiansen, M.H. (2001). Sequential learning in non-human primates. Trends Cognit. Sci. *5*, 539–546. https://doi.org/10.1016/S1364-6613(00)01800-3.

Crick, F., and Koch, C. (2003). A framework for consciousness. Nat. Neurosci. *6*, 119–126. https://doi.org/10.1038/nn0203-119.

Curry, E.W.J. (2014). A framework for generalized subspace pattern mining in high-dimensional datasets. BMC Bioinf. *15*, 355. https://doi.org/10.1186/s12859-014-0355-5.

Dalley, J.W., Everitt, B.J., and Robbins, T.W. (2011). Impulsivity, compulsivity, and top-down cognitive control. Neuron *69*, 680–694. https://doi.org/10.1016/j.neuron.2011.01.020.

Danecek, P., Auton, A., Abecasis, G., Albers, C.A., Banks, E., DePristo, M.A., Handsaker, R.E., Lunter, G., Marth, G.T., Sherry, S.T., et al. (2011). The variant call format and VCFtools. Bioinformatics *27*, 2156–2158. https://doi.org/10.1093/bioinformatics/btr330.

De Graaf, T.A., Roebroeck, A., Goebel, R., and Sack, A.T. (2010). Brain network dynamics underlying visuospatial judgment: an FMRI connectivity study. J. Cogn. Neurosci. *22*, 2012–2026. https://doi.org/10.1162/jocn.2009.21345.

Dediu, D., and Levinson, S.C. (2018). Neanderthal language revisited: not only us. Curr. Opin. Behav. Sci. *21*, 49–55. https://doi.org/10.1016/j.cobeha.2018.01.001.

Dekleva, M., Dufour, V., de Vries, H., Spruijt, B.M., and Sterck, E.H.M. (2011). Chimpanzees (Pan troglodytes) fail a what-where-when task but find rewards by using a location-based association strategy. PLoS One *6*, e16593. https://doi.org/10.1371/journal.pone.0016593.

DeSalle, R., and Tattersall, I. (2018). What aDNA can (and cannot) tell us about the emergence of language and speech. J. Lang. Evol. *3*, 59–66. https://doi.org/10.1093/jole/lzx018.

Di Lullo, E., and Kriegstein, A.R. (2017). The use of brain organoids to investigate neural development and disease. Nat. Rev. Neurosci. *18*, 573–584. https://doi.org/10.1038/nrn.2017.107.

Ding, S.L., Royall, J.J., Sunkin, S.M., Ng, L., Facer, B.A.C., Lesnar, P., Guillozet-Bongaarts, A., McMurray, B., Szafer, A., Dolbeare, T.A., et al. (2016). Comprehensive cellular-resolution atlas of the adult human brain. J. Comp. Neurol. *524*, Spc1. https://doi.org/10.1002/cne.24097.

Doan, R.N., Bae, B.I., Cubelos, B., Chang, C., Hossain, A.A., Al-Saad, S., Mukaddes, N.M., Oner, O., Al-Saffar, M., Balkhy, S., et al. (2016). Mutations in human accelerated regions disrupt cognition and social behavior. Cell *167*, 341–354.e12.

Dorus, S., Vallender, E.J., Evans, P.D., Anderson, J.R., Gilbert, S.L., Mahowald, M., Wyckoff, G.J., Malcom, C.M., and Lahn, B.T. (2004). Accelerated evolution of nervous system genes in the origin of Homo sapiens. Cell *119*, 1027–1040. https://doi.org/10.1016/j.cell.2004.11.040.

Drummond, A.J., and Rambaut, A. (2007). BEAST: Bayesian evolutionary analysis by sampling trees. BMC Evol. Biol. *7*, 214. https://doi.org/10.1186/1471-2148-7-214.

Du, A., Zipkin, A.M., Hatala, K.G., Renner, E., Baker, J.L., Bianchi, S., Bernal, K.H., and Wood, B.A. (2018). Pattern and process in hominin brain size evolution are scale dependent. Proc. R. Soc. B Biol. Sci. *285*, 20172738. https://doi.org/10.1098/rspb.2017.2738.

Duret, L., and Mouchiroud, D. (2000). Determinants of substitution rates in mammalian genes: expression pattern affects selection intensity but not mutation rate. Mol. Biol. Evol. *17*, 68–070. https://doi.org/10.1093/oxfordjournals.molbev.a026239.

Ebersberger, I., Galgoczy, P., Taudien, S., Taenzer, S., Platzer, M., and Von Haeseler, A. (2007). Mapping human genetic ancestry. Mol. Biol. Evol. *24*, 2266–2276. https://doi.org/10.1093/molbev/msm156.

Enard, W., Przeworski, M., Fisher, S.E., Lai, C.S.L., Wiebe, V., Kitano, T., Monaco, A.P., and Pääbo, S. (2002). Molecular evolution of FOXP2, a gene involved in speech and language. Nature *418*, 869–872. https://doi.org/10.1038/nature01025.

Falkner, S., Grade, S., Dimou, L., Conzelmann, K.-K., Bonhoeffer, T., Götz, M., and Hübener, M. (2016). Transplanted embryonic neurons integrate into adult neocortical circuits. Nature *539*, 248–253. https://doi.org/10.1038/nature20113.

Fang, P., Zeng, L.L., Shen, H., Wang, L., Li, B., Liu, L., and Hu, D. (2012). Increased cortical-limbic anatomical network connectivity in major depression revealed by diffusion tensor imaging. PLoS One *7*, e45972. https://doi.org/10.1371/journal.pone.0045972.

Felleman, D.J., and Van Essen, D.C. (1991). Distributed hierarchical processing in the primate cerebral cortex. Cerebr. Cortex *1*, 1–47. https://doi.org/10.1093/cercor/1.1.1.

Ferri, F., Frassinetti, F., Ardizzi, M., Costantini, M., and Gallese, V. (2012). A sensorimotor network for the bodily self. J. Cogn. Neurosci. *24*, 1584–1595. https://doi.org/10.1162/jocn_a_00230.

Florio, M., Albert, M., Taverna, E., Namba, T., Brandl, H., Lewitus, E., Haffner, C., Sykes, A., Wong, F.K., Peters, J., et al. (2015). Human-specific gene ARHGAP11B promotes basal progenitor amplification and neocortex expansion. Science *347*, 1465–1470. https://doi.org/10.1126/science.aaa1975.

Friederici, A.D. (2017). Evolution of the neural language network. Psychon. Bull. Rev. *24*, 41–47. https://doi.org/10.3758/s13423-016-1090-x.

Fu, W., and Akey, J.M. (2013). Selection and adaptation in the human genome. Annu. Rev. Genom. Hum. Genet. *14*, 467–489. https://doi.org/10.1146/annurev-genom-091212-153509.

Ganglberger, F., Kaczanowska, J., Penninger, J.M., Hess, A., Bühler, K., and Haubensak, W. (2018). Predicting functional neuroanatomical maps from fusing brain networks with genetic information. Neuroimage *170*, 113–120. https://doi.org/10.1016/j.neuroimage.2017.08.070.

Ganglberger, F., Swoboda, N., Frauenstein, L., Kaczanowska, J., Haubensak, W., and Bühler, K. (2019). BrainTrawler: a visual analytics framework for iterative exploration of heterogeneous big brain data. Comput. Graph. *82*, 304–320. https://doi.org/10.1016/j.cag.2019.05.032.

Genty, E., Breuer, T., Hobaiter, C., and Byrne, R.W. (2009). Gestural communication of the Gorilla (Gorilla Gorilla): repertoire, intentionality and possible origins. Anim. Cognit. *12*, 527–546. https://doi.org/10.1007/s10071-009-0213-4.

Ghoussaini, M., Mountjoy, E., Carmona, M., Peat, G., Schmidt, E.M., Hercules, A., Fumis, L., Miranda, A., Carvalho-Silva, D., Buniello, A., et al. (2021). Open Targets Genetics: systematic identification of trait-associated genes using large-scale genetics and functional genomics. Nucleic Acids Res. *49*, D1311–D1320. https://doi.org/10.1093/nar/gkaa840.

Gibbs, R.A., Rogers, J., Katze, M.G., Bumgarner, R., Weinstock, G.M., Mardis, E.R., Remington, K.A., Strausberg, R.L., Venter, J.C., Wilson, R.K., et al. (2007). Evolutionary and biomedical insights from the rhesus macaque genome. Science *316*, 222–234. https://doi.org/10.1126/science.1139247.

González-Forero, M., and Gardner, A. (2018). Inference of ecological and social drivers of human brain-size evolution. Nature *557*, 554–557. https://doi.org/10.1038/s41586-018-0127-x.

Grant, S.G.N. (2016). The molecular evolution of the vertebrate behavioural repertoire. Philos. Trans. R. Soc. B Biol. Sci. *371*, 20150051. https://doi.org/10.1098/rstb.2015.0051.

Green, R.E., Krause, J., Briggs, A.W., Maricic, T., Stenzel, U., Kircher, M., Patterson, N., Li, H., Zhai, W., Fritz, M.H.-Y., et al. (2010). A draft sequence of the neandertal genome. Science *328*, 710–722. https://doi.org/10.1126/science.1188021.

Green, T.A., Alibhai, I.N., Unterberg, S., Neve, R.L., Ghose, S., Tamminga, C.A., and Nestler, E.J. (2008). Induction of activating transcription factors (ATFs) ATF2, ATF3, and ATF4 in the nucleus accumbens and their regulation of emotional behavior. J. Neurosci. *28*, 2025–2032. https://doi.org/10.1523/jneurosci.5273-07.2008.

Halligan, D.L., Kousathanas, A., Ness, R.W., Harr, B., Eöry, L., Keane, T.M., Adams, D.J., and Keightley, P.D. (2013). Contributions of protein-coding and regulatory change to adaptive molecular evolution in murid rodents. PLoS Genet. *9*, e1003995. https://doi.org/10.1371/journal.pgen.1003995.

Hanks, T.D., and Summerfield, C. (2017). Perceptual decision making in rodents, monkeys, and humans. Neuron *93*, 15–31. https://doi.org/10.1016/j.neuron.2016.12.003.

Hawrylycz, M., Miller, J.A., Menon, V., Feng, D., Dolbeare, T., Guillozet-Bongaarts, A.L., Jegga, A.G., Aronow, B.J., Lee, C.K., Bernard, A., et al. (2015). Canonical genetic signatures of the adult human brain. Nat. Neurosci. *18*, 1832–1844. https://doi.org/10.1038/nn.4171.

Hawrylycz, M.J., Lein, E.S., Guillozet-Bongaarts, A.L., Shen, E.H., Ng, L., Miller, J.A., van de Lagemaat, L.N., Smith, K.A., Ebbert, A., Riley, Z.L., et al. (2012). An anatomically comprehensive atlas of the adult human brain transcriptome. Nature *489*, 391–399. https://doi.org/10.1038/nature11405.

Haygood, R., Fedrigo, O., Hanson, B., Yokoyama, K.D., and Wray, G.A. (2007). Promoter regions of many neural- and nutrition-related genes have experienced positive selection during human evolution. Nat. Genet. *39*, 1140–1144. https://doi.org/10.1038/npre.2007.69.1.

He, Z., Han, D., Efimova, O., Guijarro, P., Yu, Q., Oleksiak, A., Jiang, S., Anokhin, K., Velichkovsky, B., Grünewald, S., et al. (2017). Comprehensive transcriptome analysis of neocortical layers in humans, chimpanzees, and macaques. Nat. Neurosci. *20*, 886–895. https://doi.org/10.1038/nn.4548.

Hecht, E.E., Murphy, L.E., Gutman, D.A., Votaw, J.R., Schuster, D.M., Preuss, T.M., Orban, G.A., Stout, D., and Parr, L.A. (2013). Differences in neural activation for object-directed grasping in chimpanzees and humans. J. Neurosci. *33*, 14117–14134. https://doi.org/10.1523/JNEUROSCI.2172-13.2013.

Herculano-Houzel, S. (2012). The remarkable, yet not extraordinary, human brain as a scaled-up primate brain and its associated cost. Proc. Natl. Acad. Sci. USA *109*, 10661–10668. https://doi.org/10.1073/pnas.1201895109.

Herculano-Houzel, S., Collins, C.E., Wong, P., and Kaas, J.H. (2007). Cellular scaling rules for primate brains. Proc. Natl. Acad. Sci. USA *104*, 3562–3567. https://doi.org/10.1073/pnas.0611396104.

Herrmann, E., Call, J., Hernández-Lloreda, M.V., Hare, B., and Tomasello, M. (2007). Humans have evolved specialized skills of social cognition: the cultural intelligence hypothesis. Science *317*, 1360–1366. https://doi.org/10.1126/science.1146282.

Hill, K., Barton, M., and Hurtado, A.M. (2009). The emergence of human uniqueness: characters underlying behavioral modernity. Evol. Anthropol. Issues News Rev. *18*, 187–200. https://doi.org/10.1002/evan.20224.

Hoffecker, J.F. (2018). The complexity of neanderthal technology. Proc. Natl. Acad. Sci. USA *115*, 1959–1961. https://doi.org/10.1073/pnas.1800461115.

Hoffmann, D.L., Standish, C.D., García-Diez, M., Pettitt, P.B., Milton, J.A., Zilhão, J., Alcolea-González, J.J., Cantalejo-Duarte, P., Collado, H., de Balbin, R., et al. (2018). U-Th dating of carbonate crusts reveals neandertal origin of iberian cave art. Science *359*, 912–915. https://doi.org/10.1126/science.aap7778.

Hofman, M.A. (2014). Evolution of the human brain: when bigger is better. Front. Neuroanat. *8*, 15. https://doi.org/10.3389/fnana.2014.00015.

Hu, Y., Marwick, B., Zhang, J.-F., Rui, X., Hou, Y.-M., Yue, J.-P., Chen, W.-R., Huang, W.-W., and Li, B. (2019). Late middle pleistocene levallois stone-tool technology in southwest China. Nature *565*, 82–85. https://doi.org/10.1038/s41586-018-0710-1.

Hughes, A.L. (2012). Evolution of adaptive phenotypic traits without positive Darwinian selection. Heredity *108*, 347–353. https://doi.org/10.1038/hdy.2011.97.

Hunt, B.G., Ometto, L., Wurm, Y., Shoemaker, D.W., Yi, S.V., Keller, L., and Goodisman, M.A.D. (2011). Relaxed selection is a precursor to the evolution of phenotypic plasticity. Proc. Natl. Acad. Sci. USA *108*, 15936–15941. https://doi.org/10.1073/pnas.1104825108.

Hunt, S.E., McLaren, W., Gil, L., Thormann, A., Schuilenburg, H., Sheppard, D., Parton, A., Armean, I.M., Trevanion, S.J., Flicek, P., et al. (2018). Ensembl variation resources. Database, bay119.

Imura, T., and Tomonaga, M. (2013). Differences between chimpanzees and humans in visual temporal integration. Sci. Rep. *19*, 3256. https://doi.org/10.1038/srep03256.

Isler, K., Christopher Kirk, E., Joseph, M., Miller, A., Albrecht, G.A., Gelvin, B.R., and Martin, R.D. (2008). Endocranial volumes of primate species: scaling analyses using a comprehensive and reliable data set. J. Hum. Evol. *55*, 967–978. https://doi.org/10.1016/j.jhevol.2008.08.004.

Jackson, A.P., Eastwood, H., Bell, S.M., Adu, J., Toomes, C., Carr, I.M., Roberts, E., Hampshire, D.J., Crow, Y.J., Mighell, A.J., et al. (2002). Identification of microcephalin, a protein implicated in determining the size of the human brain. Am. J. Hum. Genet. *71*, 136–142. https://doi.org/10.1086/341283.

Jarvis, E.D. (2019). Evolution of vocal learning and spoken language. Science *366*, 50–54.

Jaubert, J., Verheyden, S., Genty, D., Soulier, M., Cheng, H., Blamart, D., Burlet, C., Camus, H., Delaby, S., Deldicque, D., et al. (2016). Early neanderthal constructions deep in bruniquel cave in southwestern France. Nature *534*, 111–114. https://doi.org/10.1038/nature18291.

Johansson, S. (2013). The talking Neanderthals: what do fossils , genetics , and archeology say? Biolinguistics *7*, 35–74. https://doi.org/10.5964/bioling.8955.

Kaas, J.H. (2010). The evolution of sensory and motor systems in primates. In Evolution of Nervous Systems. https://doi.org/10.1016/B0-12-370878-8/00002-1.

Kalyaanamoorthy, S., Minh, B.Q., Wong, T.K.F., von Haeseler, A., and Jermiin, L.S. (2017). ModelFinder: fast model selection for accurate phylogenetic estimates. Nat. Methods *14*, 587–589. https://doi.org/10.1038/nmeth.4285.

Kano, F., Krupenye, C., Hirata, S., Tomonaga, M., and Call, J. (2019). Great apes use self-experience to anticipate an agent's action in a false-belief test. Proc. Natl. Acad. Sci. USA *116*, 20904–20909. https://doi.org/10.1073/pnas.1910095116.

Khaitovich, P., Hellmann, I., Enard, W., Nowick, K., Leinweber, M., Franz, H., Weiss, G., Lachmann, M., and Pääbo, S. (2005). Parallel patterns of evolution in the genomes and transcriptomes of humans and chimpanzees. Science *309*, 1850–1854. https://doi.org/10.1126/science.1108296.

Kirsch, L., and Chechik, G. (2016). On expression patterns and developmental origin of human brain regions. PLoS Comput. Biol. *12*, e1005064. https://doi.org/10.1371/journal.pcbi.1005064.

Kochiyama, T., Ogihara, N., Tanabe, H.C., Kondo, O., Amano, H., Hasegawa, K., Suzuki, H., Ponce de León, M.S., Zollikofer, C.P.E., Bastir, M., et al. (2018). Reconstructing the neanderthal brain using computational anatomy. Sci. Rep. *8*, 6296. https://doi.org/10.1038/s41598-018-24331-0.

Kosiol, C., Holmes, I., and Goldman, N. (2007). An empirical codon model for protein sequence evolution. Mol. Biol. Evol. *24*, 1464–1479. https://doi.org/10.1093/molbev/msm064.

Kosiol, C., Vinař, T., Da Fonseca, R.R., Hubisz, M.J., Bustamante, C.D., Nielsen, R., and Siepel, A. (2008). Patterns of positive selection in six mammalian genomes. PLoS Genet. *4*, e1000144. https://doi.org/10.1371/journal.pgen.1000144.

Krämer, A., Green, J., Pollard, J., and Tugendreich, S. (2014). Causal analysis approaches in ingenuity pathway analysis. Bioinformatics *30*, 523–530. https://doi.org/10.1093/bioinformatics/btt703.

Krupenye, C., Kano, F., Hirata, S., Call, J., and Tomasello, M. (2016). Great apes anticipate that other individuals will act according to false beliefs. Science *354*, 110–114. https://doi.org/10.1126/science.aaf8110.

Kryazhimskiy, S., and Plotkin, J.B. (2008). The population genetics of dN/dS. PLoS Genet. *4*, e1000304. https://doi.org/10.1371/journal.pgen.1000304.

Kumar, S., Stecher, G., Suleski, M., and Hedges, S.B. (2017). TimeTree: a resource for timelines, timetrees, and divergence times. Mol. Biol. Evol. *34*, 1812–1819. https://doi.org/10.1093/molbev/msx116.

Lahti, D.C., Johnson, N.A., Ajie, B.C., Otto, S.P., Hendry, A.P., Blumstein, D.T., Coss, R.G., Donohue, K., and Foster, S.A. (2009). Relaxed selection in the wild. Trends Ecol. Evol. *24*, 487–496. https://doi.org/10.1016/j.tree.2009.03.010.

Lake, B.B., Chen, S., Sos, B.C., Fan, J., Kaeser, G.E., Yung, Y.C., Duong, T.E., Gao, D., Chun, J., Kharchenko, P.V., et al. (2018). Integrative single-cell analysis of transcriptional and epigenetic states in the human adult brain. Nat. Biotechnol. *36*, 70–80. https://doi.org/10.1038/nbt.4038.

Laramée, M.E., and Boire, D. (2015). Visual cortical areas of the mouse: comparison of parcellation and network structure with primates. Front. Neural Circ. *8*, 149. https://doi.org/10.3389/fncir.2014.00149.

Lawrence, N.S., Ross, T.J., and Stein, E.A. (2002). Cognitive mechanisms of nicotine on visual attention. Neuron *36*, 539–548. https://doi.org/10.1016/s0896-6273(02)01004-8.

Leah, K. (2009). In search of a unifying theory of complex brain evolution. Ann. N. Y. Acad. Sci. *1156*, 44–67. https://doi.org/10.1111/j.1749-6632.2009.04421.x.

Lee, A., Shen, M., and Qiu, A. (2017). Psychiatric polygenic risk associates with cortical morphology and functional organization in aging. Transl. Psychiatr. *7*, 1276. https://doi.org/10.1038/s41398-017-0036-z.

Lee, J.J., Wedow, R., Okbay, A., Kong, E., Maghzian, O., Zacher, M., Nguyen-Viet, T.A., Bowers, P., Sidorenko, J., Karlsson Linnér, R., et al. (2018). Gene discovery and polygenic prediction from a genome-wide association study of educational attainment in 1.1 million individuals. Nat. Genet. *50*, 1112–1121. https://doi.org/10.1038/s41588-018-0147-3.

Lieberman, P. (2015). The evolution of language. In Handbook of Intelligence: Evolutionary Theory, Historical Perspective, and Current Concepts.

Lieberman, P. (2016). The evolution of language and thought. J. Anthropol. Sci. *94*, 127–146. https://doi.org/10.4436/jass.94029.

Lin, P., Yang, Y., Gao, J., De Pisapia, N., Ge, S., Wang, X., Zuo, C.S., Jonathan Levitt, J., and Niu, C. (2017). Dynamic default mode network across different brain states. Sci. Rep. *7*, 46088. https://doi.org/10.1038/srep46088.

Lombard, M., and Högberg, A. (2021). Four-field Co-evolutionary model for human cognition: variation in the middle stone age/middle palaeolithic. J. Archaeol. Method Theory *28*, 142–177. https://doi.org/10.1007/s10816-020-09502-6.

Löytynoja, A. (2014). Phylogeny-aware alignment with PRANK. In Multiple Sequence Alignment Methods (Totowa, NJ: Humana Press), pp. 155–170.

Lynch, M., and Conery, J.S. (2000). The evolutionary fate and consequences of duplicate genes. Science *290*, 1151–1155. https://doi.org/10.1126/science.290.5494.1151.

MacLean, E.L. (2016). Unraveling the evolution of uniquely human cognition. Proc. Natl. Acad. Sci. USA *113*, 6348–6354. https://doi.org/10.1073/pnas.1521270113.

Mantini, D., Corbetta, M., Romani, G.L., Orban, G.A., and Vanduffel, W. (2013). Evolutionarily novel functional networks in the human brain? J. Neurosci. *33*, 3259–3275. https://doi.org/10.1523/jneurosci.4392-12.2013.

Marean, C.W. (2015). An evolutionary anthropological perspective on modern human origins. Annu. Rev. Anthropol. *44*, 533–556. https://doi.org/10.1146/annurev-anthro-102313-025954.

Marinić, M., and Lynch, V.J. (2020). Relaxed constraint and functional divergence of the progesterone receptor (PGR) in the human stem-lineage. PLoS Genet. *16*, e1008666. https://doi.org/10.1371/journal.pgen.1008666.

Mattson, M.P. (2014). Superior pattern processing is the essence of the evolved human brain. Front. Neurosci. *8*, 265. https://doi.org/10.3389/fnins.2014.00265.

McDonald, J.H., and Kreitman, M. (1991). Adaptive protein evolution at the Adh locus in Drosophila. Nature *351*, 652–654. https://doi.org/10.1038/351652a0.

McKenna, A., Hanna, M., Banks, E., Sivachenko, A., Cibulskis, K., Kernytsky, A., Garimella, K., Altshuler, D., Gabriel, S., Daly, M., et al. (2010). The genome analysis toolkit: a MapReduce framework for analyzing next-generation DNA sequencing data. Genome Res. *20*, 1297–1303. https://doi.org/10.1101/gr.107524.110.

Menon, V. (2015). Salience network. In Brain Mapping: An Encyclopedic Reference.

Meyer, M., Fu, Q., Aximu-Petri, A., Glocke, I., Nickel, B., Arsuaga, J.L., Martínez, I., Gracia, A., De Castro, J.M.B., Carbonell, E., and Paabo, S. (2014). A mitochondrial genome sequence of a hominin from Sima de los Huesos. Nature *505*, 403–406. https://doi.org/10.1038/nature12788.

Meyer, M., Kircher, M., Gansauge, M.T., Li, H., Racimo, F., Mallick, S., Schraiber, J.G., Jay, F., Prüfer, K., De Filippo, C., et al. (2012). A high-coverage genome sequence from an archaic Denisovan individual. Science *338*, 222–226. https://doi.org/10.1126/science.1224344.

Mikkelsen, T.S., Hillier, L.W., Eichler, E.E., Zody, M.C., Jaffe, D.B., Yang, S.P., Enard, W., Hellmann, I., Lindblad-Toh, K., Altheide, T.K., et al. (2005). Initial sequence of the chimpanzee genome and comparison with the human genome. Nature *437*, 69–87. https://doi.org/10.1038/nature04072.

Miyata, T., and Yasunaga, T. (1980). Molecular evolution of mRNA: a method for estimating evolutionary rates of synonymous and amino acid substitutions from homologous nucleotide sequences and its application. J. Mol. Evol. *16*, 23–36. https://doi.org/10.1007/BF01732067.

Miyata, T., Kuma, K.I., Iwabe, N., and Nikoh, N. (1994). A possible link between molecular evolution and tissue evolution demonstrated by tissue specific genes. Jpn. J. Genet. *69*, 473–480. https://doi.org/10.1266/jjg.69.473.

Mizuki, Y., Takaki, M., Okahisa, Y., Sakamoto, S., Kodama, M., Ujike, H., and Uchitomi, Y. (2014). Human Rho guanine nucleotide exchange factor 11 gene is associated with schizophrenia in a Japanese population. Hum. Psychopharmacol. *29*, 552–558. https://doi.org/10.1002/hup.2435.

Mizuki, Y., Takaki, M., Sakamoto, S., Okamoto, S., Kishimoto, M., Okahisa, Y., Itoh, M., and Yamada, N. (2017). Human rho guanine nucleotide exchange factor 11 (ARHGEF11) regulates dendritic morphogenesis. Int. J. Mol. Sci. *18*, 67. https://doi.org/10.3390/ijms18010067.

Murphy, E., and Benítez-Burraco, A. (2016). Bridging the gap between genes and language deficits in schizophrenia: an oscillopathic approach. Front. Hum. Neurosci. *10*, 15. https://doi.org/10.3389/fnhum.2016.00422.

Navarrete, A., van Schaik, C.P., and Isler, K. (2011). Energetics and the evolution of human brain size. Nature *480*, 91–93. https://doi.org/10.1038/nature10629.

Nei, M. (1987). Molecular Evolutionary Genetics (Columbia University Press).

Nei, M., and Gojobori, T. (1986). Simple methods for estimating the numbers of synonymous and nonsynonymous nucleotide substitutions. Mol. Biol. Evol. *3*, 418–426. https://doi.org/10.1093/oxfordjournals.molbev.a040410.

Neubauer, S., Hublin, J.-J., and Gunz, P. (2018). The evolution of modern human brain shape. Sci. Adv. *4*, eaao5961. https://doi.org/10.1530/ey.15.14.6.

Nguyen, L.T., Schmidt, H.A., Von Haeseler, A., and Minh, B.Q. (2015). IQ-TREE: a fast and effective stochastic algorithm for estimating maximum-likelihood phylogenies. Mol. Biol. Evol. *32*, 268–274. https://doi.org/10.1093/molbev/msu300.

Nuttle, X., Giannuzzi, G., Duyzend, M.H., Schraiber, J.G., Narvaiza, I., Sudmant, P.H., Penn, O., Chiatante, G., Malig, M., Huddleston, J., et al. (2016). Emergence of a Homo sapiens-specific gene family and chromosome 16p11.2 CNV susceptibility. Nature *536*, 205–209. https://doi.org/10.1038/nature19075.

O'Connell, L.a., Hofmann, H.A.a., O'Connnell, L.A., Hofmann, H.A.a., O'Connell, L.a., and Hofmann, H.A.a. (2012). Evolution of a vertebrate social decision-making network. Science *336*, 1154–1157. https://doi.org/10.1126/science.1218889.

Ochsner, K.N., Ray, R.R., Hughes, B., McRae, K., Cooper, J.C., Weber, J., Gabrieli, J.D.E., and Gross, J.J. (2009). Bottom-up and top-down processes in emotion generation. Psychol. Sci. *20*, 1322–1331. https://doi.org/10.1111/j.1467-9280.2009.02459.x.

Ohno, S. (1970). Evolution by Gene Duplication (Berlin, Heidelberg: Springer Berlin Heidelberg).

Pääbo, S. (2014). The human condition - a molecular approach. Cell *157*, 216–226. https://doi.org/10.1016/j.cell.2013.12.036.

Pamilo, P., and Nei, M. (1988). Relationships between gene trees and species trees. Mol. Biol. Evol. *5*, 568–583. https://doi.org/10.1093/oxfordjournals.molbev.a040517.

Pandey, S., Shekhar, K., Regev, A., and Schier, A.F. (2018). Comprehensive identification and spatial mapping of habenular neuronal types using single-cell RNA-seq. Curr. Biol. *28*, 1052–1065.e7. https://doi.org/10.1016/j.cub.2018.02.040.

Parr, L.A., Waller, B.M., and Fugate, J. (2005). Emotional communication in primates: implications for neurobiology. Curr. Opin. Neurobiol. *15*, 716–720. https://doi.org/10.1016/j.conb.2005.10.017.

Pearce, E., Stringer, C., and Dunbar, R.I.M. (2013). New insights into differences in brain organization between Neanderthals and anatomically modern humans. Proc. Biol. Sci. *280*, 20130168. https://doi.org/10.1098/rspb.2013.0168.

Perez, S.I., Tejedor, M.F., Novo, N.M., and Aristide, L. (2013). Divergence times and the evolutionary radiation of new World monkeys (platyrrhini, primates): an analysis of fossil and molecular data. PLoS One *8*, e68029. https://doi.org/10.1371/journal.pone.0068029.

Posada, D. (2008). jModelTest: phylogenetic model averaging. Mol. Biol. Evol. *25*, 1253–1256. https://doi.org/10.1093/molbev/msn083.

Price, C.J. (2000). The anatomy of language: contributions from functional neuroimaging. J. Anat. *197*, 335–359. https://doi.org/10.1046/j.1469-7580.2000.19730335.x.

Prüfer, K., Racimo, F., Patterson, N., Jay, F., Sankararaman, S., Sawyer, S., Heinze, A., Renaud, G., Sudmant, P.H., De Filippo, C., et al. (2014). The complete genome sequence of a Neanderthal from the Altai Mountains. Nature *505*, 43–49. https://doi.org/10.1038/nature12886.

Quinlan, A.R., and Hall, I.M. (2010). BEDTools: a flexible suite of utilities for comparing genomic features. Bioinformatics *26*, 841–842. https://doi.org/10.1093/bioinformatics/btq033.

Rambaut, A., and Drummond, A.J. (2007). Tracer v1.4. Encycl. Atmos. Sci.

Reich, D., Green, R.E., Kircher, M., Krause, J., Patterson, N., Durand, E.Y., Viola, B., Briggs, A.W., Stenzel, U., Johnson, P.L.F., et al. (2010). Genetic history of an archaic hominin group from Denisova cave in Siberia. Nature *468*, 1053–1060. https://doi.org/10.1038/nature09710.

Richiardi, J., Altmann, A., Milazzo, A.-C., Chang, C., Chakravarty, M.M., Banaschewski, T., Barker, G.J., Bokde, A.L.W., Bromberg, U., Buchel, C., et al.; IMAGEN consortium (2015). Correlated gene expression supports synchronous activity in brain networks. Science *348*, 1241–1244. https://doi.org/10.1126/science.1255905.

Rilling, J.K., Glasser, M.F., Preuss, T.M., Ma, X., Zhao, T., Hu, X., and Behrens, T.E.J. (2008). The evolution of the arcuate fasciculus revealed with comparative DTI. Nat. Neurosci. *11*, 426–428. https://doi.org/10.1038/nn2072.

Robinson, D.L., Goldberg, M.E., and Stanton, G.B. (1978). Parietal association cortex in the primate: sensory mechanisms and behavioral modulations. J. Neurophysiol. *41*, 910–932. https://doi.org/10.1152/jn.1978.41.4.910.

Romero, I.G., Ruvinsky, I., and Gilad, Y. (2012). Comparative studies of gene expression and the evolution of gene regulation. Nat. Rev. Genet. *13*, 505–516. https://doi.org/10.1038/nrg3229.

Roth, G. (2015). Convergent evolution of complex brains and high intelligence. Philos. Trans. R. Soc. B Biol. Sci. *370*, 20150049. https://doi.org/10.1098/rstb.2015.0049.

Roth, G., and Dicke, U. (2005). Evolution of the brain and intelligence. Trends Cognit. Sci. *9*, 250–257. https://doi.org/10.1016/j.tics.2005.03.005.

Sabeti, P.C., Reich, D.E., Higgins, J.M., Levine, H.Z.P., Richter, D.J., Schaffner, S.F., Gabriel, S.B., Platko, J.V., Patterson, N.J., McDonald, G.J., et al. (2002). Detecting recent positive selection in the human genome from haplotype structure. Nature *419*, 832–837. https://doi.org/10.1038/nature01140.

Salmi, R., Presotto, A., Scarry, C.J., Hawman, P., and Doran-Sheehy, D.M. (2020). Spatial cognition in western Gorillas (Gorilla Gorilla): an analysis of distance, linearity, and speed of travel routes. Anim. Cognit. *23*, 545–557. https://doi.org/10.1007/s10071-020-01358-3.

Schreurs, B.G. (2010). The effects of cholesterol on learning and memory. Neurosci. Biobehav. Rev. *34*, 1366–1379. https://doi.org/10.1016/j.neubiorev.2010.04.010.

Seeley, W.W., Menon, V., Schatzberg, A.F., Keller, J., Glover, G.H., Kenna, H., Reiss, A.L., and Greicius, M.D. (2007). Dissociable intrinsic connectivity networks for salience processing and executive control. J. Neurosci. *27*, 2349–2356. https://doi.org/10.1523/jneurosci.5587-06.2007.

Semendeferi, K., and Damasio, H. (2000). The brain and its main anatomical subdivisions in living hominoids using magnetic resonance imaging. J. Hum. Evol. *38*, 317–332. https://doi.org/10.1006/jhev.1999.0381.

Sherwood, C.C., Subiaul, F., and Zawidzki, T.W. (2008). A natural history of the human mind: tracing evolutionary changes in brain and cognition. J. Anat. *212*, 426–454. https://doi.org/10.1111/j.1469-7580.2008.00868.x.

Shi, L., Luo, X., Jiang, J., Chen, Y., Liu, C., Hu, T., Li, M., Lin, Q., Li, Y., Huang, J., et al. (2019). Transgenic rhesus monkeys carrying the human MCPH1 gene copies show human-like neoteny of brain development. Natl. Sci. Rev. *6*, 480–493. https://doi.org/10.1093/nsr/nwz043.

Shimodaira, H. (2002). An approximately unbiased test of phylogenetic tree selection. Syst. Biol. *51*, 492–508. https://doi.org/10.1080/10635150290069913.

Silcox, M.T., Dalmyn, C.K., and Bloch, J.I. (2009). Virtual endocast of ignacius graybullianus (paromomyidae, primates) and brain evolution in early primates. Proc. Natl. Acad. Sci. USA *106*, 10987–10992. https://doi.org/10.1073/pnas.0812140106.

Sliwa, J., and Freiwald, W.A. (2017). A dedicated network for social interaction processing in the primate brain. Science *356*, 745–749. https://doi.org/10.1126/science.aam6383.

Smith, S.M., Fox, P.T., Miller, K.L., Glahn, D.C., Fox, P.M., Mackay, C.E., Filippini, N., Watkins, K.E., Toro, R., Laird, A.R., et al. (2009). Correspondence of the brain's functional architecture during activation and rest. Proc. Natl. Acad. Sci. USA *106*, 13040–13045. https://doi.org/10.1073/pnas.0905267106.

Smith, J.B., Watson, G.D.R., Liang, Z., Liu, Y., Zhang, N., and Alloway, K.D. (2019). A Role for the Claustrum in Salience Processing? Front Neuroanat. *13*, 64.

Snell-Rood, E.C., Van Dyken, J.D., Cruickshank, T., Wade, M.J., and Moczek, A.P. (2010). Toward a population genetic framework of developmental evolution: the costs, limits, and consequences of phenotypic plasticity. Bioessays *32*, 71–81. https://doi.org/10.1002/bies.200900132.

Sousa, A.M.M., Meyer, K.A., Santpere, G., Gulden, F.O., and Sestan, N. (2017). Evolution of the human nervous system function, structure, and development. Cell *170*, 226–247. https://doi.org/10.1016/j.cell.2017.06.036.

Stuart, T., Butler, A., Hoffman, P., Hafemeister, C., Papalexi, E., Mauck, W.M., Hao, Y., Stoeckius, M., Smibert, P., and Satija, R. (2019). Comprehensive integration of single-cell data. Cell *177*, 1888–1902.e21. https://doi.org/10.1016/j.cell.2019.05.031.

Tang, K., Thornton, K.R., and Stoneking, M. (2007). A new approach for using genome scans to detect recent positive selection in the human genome. PLoS Biol. *5*, e171. https://doi.org/10.1371/journal.pbio.0050171.

Tattersall, I. (2017). The material record and the antiquity of language. Neurosci. Biobehav. Rev. *81*, 247–254. https://doi.org/10.1016/j.neubiorev.2017.01.043.

Tavor, I., Jones, O.P., Mars, R.B., Smith, S.M., Behrens, T.E., and Jbabdi, S. (2016). Task-free MRI predicts individual differences in brain activity during task performance. Science *352*, 216–220. https://doi.org/10.1126/science.aad8127.

Templeton, A.R. (2008). The reality and importance of founder speciation in evolution. Bioessays *30*, 470–479. https://doi.org/10.1002/bies.20745.

Thannickal, T.C., Moore, R.Y., Nienhuis, R., Ramanathan, L., Gulyani, S., Aldrich, M., Cornford, M., and Siegel, J.M. (2000). Reduced number of hypocretin neurons in human narcolepsy. Neuron *27*, 469–474. https://doi.org/10.1016/s0896-6273(00)00058-1.

Tremblay, S., Sharika, K.M., and Platt, M.L. (2017). Social decision-making and the brain: a comparative perspective. Trends Cognit. Sci. *21*, 265–276. https://doi.org/10.1016/j.tics.2017.01.007.

Trujillo, C.A., Rice, E.S., Schaefer, N.K., Chaim, I.A., Wheeler, E.C., Madrigal, A.A., Buchanan, J., Preissl, S., Wang, A., Negraes, P.D., et al. (2021). Reintroduction of the archaic variant of NOVA1 in cortical organoids alters neurodevelopment. Science *371*, eaax2537. https://doi.org/10.1126/science.aax2537.

Tuller, T., Kupiec, M., and Ruppin, E. (2008). Evolutionary rate and gene expression across different brain regions. Genome Biol. *9*, 1422–R211. https://doi.org/10.1186/gb-2008-9-9-r142.

Uddin, L.Q., and Uddin, L.Q. (2017). Anatomy of the salience network. Salience Netw. Hum. Brain, 5–10. https://doi.org/10.1016/b978-0-12-804593-0.00002-3.

Ullman, M.T. (2004). Contributions of memory circuits to language: the declarative/procedural model. Cognition *92*, 231–270. https://doi.org/10.1016/j.cognition.2003.10.008.

Urgesi, C., Aglioti, S.M., Skrap, M., and Fabbro, F. (2010). The spiritual brain: selective cortical lesions modulate human self-transcendence. Neuron *65*, 309–319. https://doi.org/10.1016/j.neuron.2010.01.026.

Vai, B., Sferrazza Papa, G., Poletti, S., Radaelli, D., Donnici, E., Bollettini, I., Falini, A., Cavallaro, R., Smeraldi, E., and Benedetti, F. (2015). Abnormal cortico-limbic connectivity during emotional processing correlates with symptom severity in schizophrenia. Eur. Psychiatry *30*, 590–597. https://doi.org/10.1016/j.eurpsy.2015.01.002.

Van Der Lee, R., Wiel, L., Van Dam, T.J.P., and Huynen, M.A. (2017). Genome-scale detection of positive selection in nine primates predicts human-virus evolutionary conflicts. Nucleic Acids Res. *45*, 10634–10648. https://doi.org/10.1093/nar/gkx704.

Van Essen, D.C., Smith, S.M., Barch, D.M., Behrens, T.E.J., Yacoub, E., and Ugurbil, K. (2013). The Wu-minn human connectome project: an overview. Neuroimage *80*, 62–79.

Villanueva-Cañas, J.L., Laurie, S., and Albà, M.M. (2013). Improving genome-wide scans of positive selection by using protein isoforms of similar length. Genome Biol. Evol. *5*, 457–467.

Vossel, S., Geng, J.J., and Fink, G.R. (2014). Dorsal and Ventral Attention Systems: distinct neural circuits but collaborative roles. Neuroscientist *20*, 150–159.

Wang, G.Z., Belgard, T.G., Mao, D., Chen, L., Berto, S., Preuss, T.M., Lu, H., Geschwind, D.H., and Konopka, G. (2015). Correspondence between resting-state activity and brain gene expression. Neuron *88*, 659–666. https://doi.org/10.1016/j.neuron.2015.10.022.

Wang, J., Bruford, M.W., Zhan, X., Pan, S., Wang, J., Dixon, A., He, J., Muller, M.G., Liu, Y., Ni, P., et al. (2013). Peregrine and saker falcon genome sequences provide insights into evolution of a predatory lifestyle. Nat. Genet. *45*, 563–566. https://doi.org/10.1038/ng.2588.

Weyrich, L.S., Soubrier, J., Arriola, L., Llamas, B., Breen, J., Alt, K.W., Caramelli, D., Dresely, V., Farrell, M., Farrer, A.G., et al. (2017). Neanderthal behaviour, diet, and disease inferred from ancient DNA in dental calculus. Nature *544*, 357–361. https://doi.org/10.1038/nature21674.

Whiten, A. (2000). Primate culture and social learning. Cognit. Sci. *24*, 477–508. https://doi.org/10.1207/s15516709cog2403_6.

Whittingstall, K., Bernier, M., Houde, J.C., Fortin, D., and Descoteaux, M. (2014). Structural network underlying visuospatial imagery in humans. Cortex *56*, 85–98. https://doi.org/10.1016/j.cortex.2013.02.004.

Wilson, B., and Petkov, C.I. (2011). Communication and the primate brain: insights from neuroimaging studies in humans, chimpanzees and macaques. Hum. Biol. *83*, 175–189. https://doi.org/10.3378/027.083.0203.

Wynn, T. (1998). Did Homo erectus speak? Camb. Archaeol. J. *8*, 78–81.

Wynn, T., and Coolidge, F.L. (2004). The expert neandertal mind. J. Hum. Evol. *46*, 467–487. https://doi.org/10.1016/j.jhevol.2004.01.005.

Yang, Z. (1998). Likelihood ratio tests for detecting positive selection and application to primate lysozyme evolution. Mol. Biol. Evol. *15*, 568–573. https://doi.org/10.1093/oxfordjournals.molbev.a025957.

Yang, Z. (2007). Paml 4: phylogenetic analysis by maximum likelihood. Mol. Biol. Evol. *24*, 1586–1591. https://doi.org/10.1093/molbev/msm088.

Yang, Z., and Nielsen, R. (1998). Synonymous and nonsynonymous rate variation in nuclear genes of mammals. J. Mol. Evol. *46*, 409–418. https://doi.org/10.1007/PL00006320.

Zanto, T.P., and Gazzaley, A. (2013). Fronto-parietal network: flexible hub of cognitive control. Trends Cognit. Sci. *17*, 602–603. https://doi.org/10.1016/j.tics.2013.10.001.

Zerbino, D.R., Achuthan, P., Akanni, W., Amode, M.R., Barrell, D., Bhai, J., Billis, K., Cummins, C., Gall, A., Girón, C.G., et al. (2018). Ensembl 2018. Nucleic Acids Res. *46*, D754–D761. https://doi.org/10.1093/nar/gkx1098.

Zhong, M., Lange, K., Papp, J.C., and Fan, R. (2010). A powerful score test to detect positive selection in genome-wide scans. Eur. J. Hum. Genet. *18*, 1148–1159. https://doi.org/10.1038/ejhg.2010.60.

STAR★METHODS

KEY RESOURCES TABLE

REAGENT or RESOURCE	SOURCE	IDENTIFIER
Deposited data		
Sequence data *Mus musculus* *Otolemur garnetti* *Callithrix jacchus* *Macaca mulatta* *Nomascus leucogenys* *Pan troglodytes* *Gorilla gorilla* *Homo sapiens*	OMA orthology database	https://omabrowser.org/oma/home/
Sequence data *Homo Denisovan*	Max Planck Institute for Evolutionary Anthropology	http://cdna.eva.mpg.de/denisova/VCF/hg19_1000g/
Sequence data *Homo neanderthalensis*	Max Planck Institute for Evolutionary Anthropology	http://cdna.eva.mpg.de/denisova/VCF/hg19_1000g/
Human brain gene expression pattern	Allen Human Brain Atlas (ABA)	https://human.brain-map.org/
Task-evoked functional brain activity maps (FNs)	Human Connectome Project (HCP)	www.humanconnectome.org
Functional genetic annotations	Ingenuity Pathway Analysis (IPA)	https://www.qiagenbioinformatics.com/products/ingenuitypathway-analysis
Genetic associations	OpenTargets database	https://platform.opentargets.org/
Software and algorithms		
GABi: Genetic Algorithm for Generalized Biclustering	Curry, 2014	https://rdrr.io/cran/GABi/man/GABi.html
Predicting functional neuroanatomical maps from fusing brain networks with genetic information	Ganglberger et al., 2018	https://github.com/NeuroscienceTools/GWCA
BrainTrawler	Ganglberger et al., 2019	https://doi.org/10.1016/j.cag.2019.05.032

RESOURCE AVAILABILITY

Lead contact

For further information and resource requests, please contact Wulf Haubensak (wulf.haubensak@meduniwien.ac.at).

Materials availability

This study did not generate new unique reagents.

Data and code availability

Sources associated with published data are listed in the key resources table and referenced in the STAR Methods. All data generated in the preparation of this manuscript are included in Tables S2, S3, S4, S5, S6, S7 and Data S1.

The code used to compute the evolutionary genetic data is described in the STAR Methods and included in Data S5. The code developed for building the computational neuroanatomy atlas and biclusters is described in the STAR Methods and can be found in Data S6.

Any additional information required to reanalyze the data reported in this paper will be made available by the lead contact upon request.

METHOD DETAILS

Phylogenetic analysis and ω calculation

Data collection

We selected 20,787 human protein-coding genes together with their brain expression data sourced from oligo microarrays from the Allen Human Brain Atlas (Hawrylycz et al., 2012). The brain gene expression data comprise 3,702 biopsy sites across the brain.

According to the OMA orthology database (accessed on 26.03.2019; (Altenhoff et al., 2018)), among the 20,787 protein-coding genes in humans only 10,030 exhibited 1:1 orthologs in species 1-7 presented in Table S8. We collected the coding sequences for these 10,030 genes in species 1-8 presented in Table S8. If a human gene has several transcripts, only one is used for the identification of orthologs in the OMA database. Accordingly, we use only one splice variant per gene in our analysis.

Genes that correspond specifically to Denisovan and Neanderthal were reconstructed from the human coding genes as annotated in GRCh37 substituting the SNPs extracted from VCF files using VCFtools (v0.1.11; (Danecek et al., 2011)). Only high-quality SNPs (minQ = 30, minDP = 10) were mapped to the human reference genome (hg19/GRCh37) using the Genome Analysis Toolkit (GATK, v4.1.1.0; (McKenna et al., 2010)). Next, we obtained coding sequences for Denisovan and Neanderthal using bedtools (v2.28.0; (Quinlan and Hall, 2010)) and exon information (position and orientation) obtained for GRCh37 human genome assembly from Ensembl project (accessed on 26.03.2019; (Hunt et al., 2018), http://grch37.ensembl.org/index.html).

The 10,030 OMA-orthologs are based on the GRCh38 human genome assembly, whereas Denisovan and Neanderthal coding sequences were prepared using the GRCh37 assembly. Differences in annotations of the human genome assemblies led to the exclusion of 533 OMA-orthologs (some transcripts were not annotated in GRCh37, whereas other transcripts had different lengths of coding sequences reported in GRCh37 and GRCh38).

Among the remaining 9,497 ortholog genes, 4,300 genes had identical sequences in at least two of the ten species (Table S9).

Phylogenetic analysis

Population genetics theory predicts incomplete lineage sorting (ILS) for recently and rapidly diverged species; thus, a gene-tree may be different from the species-tree (Nei, 1987). ILS is well-known for the gorilla, chimp, and human species-tree, whereas three different gene-trees are compatible with the species-tree (Ebersberger et al., 2007). This is also observed for the Denisovan, Neanderthal, human triple (Meyer et al., 2014; Reich et al., 2010), where three different gene-trees are possible. In summary, this results in nine different gene-trees, coined ILS-trees (Figure S12, bottom), whereas the sub-trees comprising the five non-hominids agree with the canonical species-tree (Figure S12, top). According to population genetics theory, 105 gene-trees are compatible with the species-tree. However, we show that the ILS-trees are the most frequent and provide a compromise between considering only the species-tree or all different gene-trees.

For each gene, a multiple sequence alignment was built with PRANK (v.151120; (Löytynoja, 2014)) with the codon option, which uses the codon substitution matrix developed by Kosiol et al. (Kosiol et al., 2007). Maximum likelihood gene-trees were inferred using IQ-TREE (v1.6.10; (Nguyen et al., 2015)) using the best-fit codon model identified by ModelFinder (Kalyaanamoorthy et al., 2017). For each gene we performed five independent IQ-TREE runs to avoid getting stuck in local optima. The tree with the highest likelihood among the five runs is considered the (maximum likelihood) ML-tree.

Of 9,497 ML-trees, 6,256 agreed with one of the nine ILS-trees (Figure S12). Note, that due to short sequences and little phylogenetic information provided by multiple sequence alignment, tree reconstruction may be inaccurate. Therefore, we applied the Approximately Unbiased tree topology test (AU-test, (Shimodaira, 2002)) to the 3,241 ML-trees not compatible with any of the ILS-trees. The AU-test computes the p-value for each tree from a user-defined collection of (plausible) trees. If the p-value is larger than 0.05, the corresponding tree is not rejected and is therefore a plausible alternative to the ML-tree, which also appears in the collection.

Thus, for each gene we run the AU-test (as implemented in IQ-TREE) with ten trees: the ML-tree and the ILS-trees. According to the AU-test for only 519 genes, all ILS-trees performed significantly worse than the ML-tree. For the remaining 2,722 genes, at least one ILS-tree was not rejected. For each of the 2,722 genes we selected the gene-tree with the highest p-value among the non-rejected ILS-trees and used it instead of the ML-tree in subsequent analyses. If several trees yielded the same (maximum) p-value, one of the trees was chosen at random. This process generates a total of 8,978 gene-trees compatible with our current view of the species-tree.

To ensure that the subset of nine chosen ILS-trees (Figure S12) from the 105 possible ILS-trees is a viable alternative to ML-trees for most genes, we repeated the AU-test by analyzing a set of 106 trees: all possible 105 ILS-trees and the ML-tree. In this second analysis, at least one of the nine ILS-trees was among the alternatives (i.e., not rejected) for as many as 2,794 genes (with 2,022 cases being among the best alternatives, i.e., having the maximum p-value). For 366 genes all 105 ILS-trees were rejected and for only 81 genes all nine ILS-trees from Figure S12 were rejected, whereas some other ILS-trees were not rejected. Since only a fraction of genes could be better explained by the ILS-trees outside of the nine considered, we carried out the analysis for the aforementioned 8,978 gene-trees.

ω calculation

For each of the 8,978 gene-trees, we computed ratios of non-synonymous (dN) to synonymous (dS) nucleotide substitutions rates, ω. For each gene-tree we performed five *codeml* (implemented in PAML v4.9i, (Yang, 2007)) runs to estimate branch specific ω's (Yang, 1998; Yang and Nielsen, 1998). Specifically, for each gene-tree *codeml* computed the branch lengths (i.e., the expected numbers of nucleotide substitutions per codon) and ω for each branch in the gene-tree. For subsequent analysis, we used the gene-tree specific ω's that afforded the highest likelihood for the particular gene-tree among 5 *codeml* runs.

Due to characteristics of the data (e.g., little sequence divergence, short sequences), we worked with unstable or unreliable estimates of the ω's. We identified an ω value as unstable if its estimates varied across 5 runs by more than 10%. Moreover, we labelled an ω as unreliable if the corresponding branch length was $< 10^{-4}$.

For an overview of ω estimates for each branch we split the values into four categories: (i) filtered out values (unstable and unreliable estimates); (ii) 0 values (i.e., dN = 0); (iii) values from 0 to ∞ (i.e., dN≠0, dS≠0); and (iv) ∞ values (i.e., dS = 0). Figures S13 and S14 provide plots for each branch and Table S10 summarizes all data.

In the hominid clades, many ω values were either filtered out or were equal to zero or ∟. ,ith the exception of Branch 8 (the Denisovan branch) (see Figures S14, S13 and Table S10 for comparison). This is expected, since in general hominid species sequences are very similar to one another resulting in limited information/mutations to infer the parameters. Despite the large proportion of 0's and filtered out values, there remained many ω estimates greater than 0.

Archaic and modern humans are genetically very similar. However, there are insufficient population data for extinct species to identify polymorphic sites. Moreover, due to polymorphism within population data, positive selection can lead to smaller, but not larger, ω estimates (Kryazhimskiy and Plotkin, 2008) than without polymorphism. Therefore, this approach might underestimate positive selection in some genes (i.e., those that are exposed to polymorphism), however we still identified a sufficient number of genes with ω >1 (Figures 1B and S6), a characteristic indicator of positive selection. As such, we speculate that despite high genetic similarity between the AMH and its archaic relatives, polymorphism does not affect ω estimation of all the genes. Genes with high ω are the primary focus of this study. We also applied stringent filtering to the data and included only reliably estimated ω values in the analysis. Additionally, we reasoned that using ranked ω (see STAR Methods, Computational neuroanatomy) instead of absolute estimates mitigates the effect of potentially biased estimation due to polymorphism. Overall, ω estimation is a comparably conservative approach in the absence of population data to represent extinct species.

Phylogenetic timeline

To determine the general evolutionary relationships among the selected species and reconstruct the timing of evolutionary divergences, we reconstructed a phylogenetic tree from mitochondrial genomes using a Bayesian approach in BEAST 2.5 (Drummond and Rambaut, 2007). First, the best nucleotide substitution model was determined using JMODELTEST (Posada, 2008). We then implemented this model in BEAST. To account for variable rates of evolution among different primate lineages, we used a relaxed lognormal prior on the clock rate. We used three independent normally distributed and soft-bounded calibration priors (Perez et al., 2013) to place a timeframe onto our phylogeny. We used an AMH-chimpanzee mean divergence of 7.8 Mya (SD 1.2 Mya), and Old-World monkey-ape divergence of 28 Mya (SD 3 Mya) and lastly, we placed a 60 Mya mean (SD 2.8 Mya) time for the coalescence of all primate lineages. This fully parameterized model was run five times, each time for 200 million simulations, logging parameters every 20,000 steps, and discarding the first 20% as burn-in. MCMC convergence was assessed by viewing MCMC traces directly and by ESS values in TRACER 1.6 (Rambaut and Drummond, 2007). A maximum clade credibility tree was calculated and annotated in Figtree 1.4 (Rambaut and Drummond, 2007). The results of the mt-derived phylogeny (Figure S12) support the major gene tree topology in Figure 1A.

Note that, formally, Denisovans and Neanderthals split after the split from the human ancestor. However, mtDNA derived phylogeny and the major gene-tree topology (Figure 1A) places Neanderthal closer to AMH (Meyer et al., 2014) and support a Chimp-to-Denisovan-Neanderthal-AMH species order.

Computational neuroanatomy

Genetic data preparation

To compute the evolutionary signatures in the mammalian we used 8,978 genes (rows) x 21 branches (columns). The spatial gene expression data (oligo microarrays) for genes at 3,702 biopsy sites in the brain were downloaded from the Allen Human Brain Atlas (ABA).

We ranked-normalized ω for each branch (rank/number of genes) and omitted undefined ω (dS = 0) values (Villanueva-Cañas et al., 2013). ω values were transformed with ranked-normalized ω′s close to 1 corresponding to the largest ω′s for a given branch and a rank-normalized ω′s close to 0, indicating the lowest values (see Table S3) (Figure S16).

Task-evoked functional brain activity

Task-specific brain activity maps were downloaded from the Human Connectome Project (HCP) website (www.humanconnectome.org). We used data available for seven major domains, whose detailed descriptions can be found in Barch et al. (Barch et al., 2013). Contrasts selected for comparison with ω functional maps were collected and are presented in Table S12. The contrast labels and behavioral signature descriptions correspond to Tavor et al. (Tavor et al., 2016). To identify significant brain activity, z-scores of the task fMRI were subjected to thresholds +/− 5 (i.e., a signal within 5 sigmas from the mean was omitted) as indicated by Barch et al. (Barch et al., 2013). To compare these data with spatial gene expression data, we sampled the task fMRI data at the MNI coordinates of 3,702 biopsy sites. We visualized the results at a regional level in Figure S4 (top). Note, that this was conducted for the purpose of readability and visualization. The data are used for subsequent analyses on the original 3,702 site level.

Functional network meta-comparison

Literature-based regional comparisons involved in several functional networks were extracted from fMRI scans and correlated with functional maps (STAR Methods, Generating ω-weighted maps). The networks used in the study are presented in Table S13. To ensure the data aligned with the task fMRI and the spatial gene expression, we upsampled region-level data to the biopsy site level labeling present/absent (0/1). The region level results are depicted in Figure S4 (bottom) for readability and visualization purposes. The data are used for subsequent analysis on the original 3,702 site level.

Generating ω-weighted maps

To visualize the evolutionary landscape throughout brain's phylogenetic history, we created brain-region level evolutionary maps that color-code each region by its evolutionary timepoint. Timepoints were encoded by associating each brain region with the branch that yielded the strongest structural association of genes with high ω values.

To predict the association of genes released from strong purifying selection (high ω) with functional neuroanatomical maps, we applied a recently developed methodology (Ganglberger et al., 2018). Specifically, for internal (Branch 1-11) and external branches leading to chimp, Denisovan, Neanderthal and human we applied the corresponding rank-normalized ω to weight the spatial gene expression of 3,702 biopsy-sites from microarray data of the ABA (Hawrylycz et al., 2012). The multiplication of a gene's expression with its ω of a branch resulted in 15 (for each branch) different weightings of the input gene set. Spatial gene expression was normalized by robust z-score normalization (median and median absolute deviations in lieu of means and standard deviations) to account for sample and region effects.

To obtain the cumulative characteristic transcriptomic properties of an evolutionary branch at a biopsy-site, we aggregated the weighted spatial gene expression by computing the trimmed mean. For statistical evaluation, we compared this measure to weightings with randomly shuffled ω (n = 10000) using z-tests. The False Discovery Rate of the resulting p-values was adjusted using the Benjamini-Hochberg method (FDR = 0.1).

Finally, we combined the 15 individual selection maps into a single evolutionary map of selection history. To this end, brain regions were colored by branch with the most significant regionally-averaged p-value. Figure 2 shows the data on a regional level for readability and visualization purposes, however the data were computed on the 3,702-biopsy site level (labeled and annotated selected brain slices: Figure S2, all brain slices: Data S2). To analyze the selection pressure on brain regions over time (i.e., how biopsy site p-values changed for different branches), we performed hierarchical clustering (Ward D2 Criterion). This resulted in 8 clusters of biopsy sites (more clusters did not increase variance) that show similar timelines (Figure 3A visualizes the biopsy level data on a region level for readability). We visualized the clusters' timelines in Figure 3B, where we computed rank normalization of the $-\log_{10}$ p-values, so that values close to 1 indicate high significance (i.e., higher selection pressure), and values close to 0 indicate lower significance (i.e., lower selection pressure).

Note, that the individual maps only showed the most significant p-value of biopsy sites within a brain region (slices 9, 18, 27, 36, 45, 54, 63, 72, 81, 90, and 99 of the Allen Human Brain Atlas: atlas.brain-map.org/atlas?atlas = 265297125), since the evolutionary map was computed first at the biopsy site-level (Table S4) and then visualized on a regional level.

Given that the high conservation between closely related species yields only few genetic changes and a low numbers of high ω genes (e.g., Figure 1B, Branches 7, 'Neanderthal' and 'AMH' in recent hominin evolution), which makes their impact notoriously difficult to interpret. The workflow above used to generate these maps was specifically tuned for use in small to medium size gene sets of ~10-100 functionally-related genes (Ganglberger et al., 2018). In our case, it allowed us to probe for statistically meaningful evolutionary patterns even with only a few diverging genes between close species. Consequently, for evolutionarily-grouped gene sets, the methods yielded robust predictions for these branches, which had sufficient genetic information (Figure 1B, 'Major tree'). In contrast, less prominent side branches with too few genes (e.g., Figure 1B, 'Alt. trees') consequently did not reach significant accumulation in any brain region (Figure S2).

Subspace pattern mining for network evolution via biclustering

To identify genes linked to specific tasks or functional networks, we mined co-evolving genes with high spatial correlations to these networks. Therefore, we retrieved AMH spatial gene expression data from 3,702 biopsy sites in the ABA for each of the 8,978 genes in the ω ranked table. We mapped both the task fMRI data of 11 networks (STAR Methods, Task-evoked functional brain activity) and the literature-based data from another 11 networks (STAR Methods, Functional network meta-comparison) to the gene expression data of the biopsy sites and computed Spearman rank correlation coefficients over the 3,702 sites between every gene and network.

First, we rank-normalized the 8978 × 11 fMRI-to-gene-expression matrix and the 8978 × 11 literature-to-gene-expression matrix to allow for comparison across both types of functional data. Functional network specificity for each gene was computed by rank-normalization (rank/rank/number of networks) for each gene over all networks, so they mapped to a range between 0 and 1, where networks with the lowest correlations were set to zero and those with the highest correlations were set to a value of 1. We concatenated these data with the table of ω-ranked genes for each of the 21 evolutionary branches in the main and alternative tree topologies, resulting in an 8978 × 43 spatio-temporal network table (Table S7). For this table, we set correlation value for genes with a low overall correlation with all networks (i.e., < 0.1) to 0.

Next, we mined both these data tables in R using GABi (Curry, 2014), a framework that facilitates a genetic algorithm for biclustering rows and columns of a matrix simultaneously. Compared to other biclustering algorithms, GABi allows for the definition of customized bicluster properties, such as coherence, consistency, and size. We used these custom criteria, also called the "fitness function", to identify biclusters of highly selected genes (e.g., genes that have high ω ranks over multiple branches) with high specificity for similar functional networks (e.g., genes with high network correlation ranks for the same networks). Therefore, GABi creates a set of candidate solutions (i.e., a set of genes) and applies the fitness function to determine the branches and networks that fit the custom criteria. The algorithm iteratively optimizes the candidate solutions to find the largest bicluster fitting these criteria by means of evolution-inspired operators such as mutation, crossover, and selection (Curry, 2014). We defined the following custom criteria for the fitness function to identify the largest bicluster:

1. with at least one branch and one network, since biclusters without one of these criteria do not represent genes with high ω ranks and high specificity for similar functional networks
2. with branches with an ω rank $\geq$0.9 for genes in the bicluster. This selects only genes that have branches with an ω rank above or equal to 0.9, putting them in the upper 10^{th} percentile of ω ranks. Therefore, they are considered the top 10 percent of genes with the highest selection pressure. We applied the criteria also with an ω rank $\leq$0.1 to obtain biclusters with low selection pressure (Table S5).
3. with networks with a mean network correlation specificity rank $\geq$0.75 for genes in the bicluster. Therefore, only genes with a network specificity in the top 25% (i.e., the networks with the 1-5th highest correlation with each gene) were present in the bicluster (Table S5).

If a bicluster has these properties, we defined its fitness as:

$$\text{fitness} = r^{*}\left(c_{\omega}^{*}w_{\omega} + c_{\text{network}}{}^{*}w_{\text{network}}\right)$$

where r is the number of rows, c_{ω} the amount of ω rank columns. c_{network} is the amount of gene-to-network correlation rank columns that have not yet been assigned to another bicluster. This ensures that the GABi algorithm looks for the largest biclusters for every network in subsequent iterations. For more information, see the usage of "tabu-lists" in (Curry, 2014). w_{ω} and w_{network} are weighting factors to account for different amounts of ω rank columns (21) and network correlation rank columns (22). Otherwise, it is more likely to identify biclusters with network correlation rank columns than ω rank columns. For ω-network biclustering, w_{ω} = 1.024 and w_{network} = 0.977 sum up to 43 (21 + 22) again. Therefore, the columns count in total the same as for an unweighted approach, but individually ω rank columns count more than network columns.

To account for the large proportion of filtered out values (category i), 0's (category ii) and ∞ values (category iv) (see STAR Methods, ω calculation for details), we replaced c_{ω} with ω_{valid}, where ω_{valid} is a vector of the relative number of valid values per ω rank column. Otherwise, branches with only a few valid values (i.e., values that do not fall into the defined categories) would be underrepresented in the biclustering since the fitness function would be tailored to find the largest biclusters (=most rows and columns). We also included 0's (category ii) to find biclusters with low selection pressure (Figure S6).

Stability tests were performed on random subsets of data to empirically estimate parameters for the genetic algorithm utilized by GABi. We found that a population size of at least 100 times the 'chromosome' length (the number of rows of the data set (Curry, 2014)) with ~10000 demes (separate subpopulations) led to stable results, reproducible over multiple runs. This number of demes was necessary to minimize the chances of locally optimal biclustering solutions since it must converge to solutions that are relatively small compared to the search space. Identified biclusters accounted for approximately 0.1-1% of the total number of genes.

We carried out biclustering with these parameters 4 times with similar results. All biclusters presented in this paper had at least 90% similar genes, and 90% of the biclusters had 100% similar genes. The statistical evaluation was performed using permutation tests to verify that the biclusters had significantly higher mean ω ranks and gene-to-network correlation ranks compared to random sets of a similar size. p-values were highly significant (<0.0001), which was expected since the fitness function was specifically designed to pinpoint biclusters with high ω ranks (therefore, these data are not shown).

Biclusters are depicted in Figures 4 and 6, and were visualized using BrainTrawler (Ganglberger et al., 2019). Nodes were selected from the bicluster's networks (Tables S12, S6, Figure S4), and the edges represented the strongest spatial gene expression correlation of the bicluster's genes. The networks were created similarly to STAR Methods; Subspace pattern mining for network evolution via biclustering. Originally, the edges showed a region-bias (i.e., regions with higher correlations between them compared to others over the entire network) due to the number of genes within a bicluster (the correlation of gene sets converges to the genome-wide spatial gene expression correlation with increasing size). We targeted this by generating an empirical distribution for each individual edge using 1000 random drawn gene sets from the genome (of the same size as the bicluster). These distributions (i.e., their mean and standard distribution) were used for z-score normalization of the bicluster edges. Summarized biclustering results and statistics for full lineage and hominids are available in Table S5.

Single-cell gene expression for cortical brain regions

Single-cell gene expression data across 3 brain regions (BA9/superior frontal gyrus – SFG, visual cortex/cuneus - CUN, cerebellar cortex - CbCx) for 33 cell type clusters were used (from Lake et al., 2018). Not all 33 cell types were present in all brain regions, leading to 61 cell type/brain region combinations. The raw unique molecular identifier (UMI) count matrix (genes x single-cell samples) was normalized to logCPM (logarithmic counts per million reads). We filtered for biological variability of genes by applying a threshold to the coefficient of variation over multiple samples (Pandey et al., 2018). Cell-cell variation factors (i.e., the percentage of mtRNA, batch effect) were regressed out according to the Seurat R package (scaleData function) (Stuart et al., 2019). We matched the genes of this data with the ω ranked table, generating an 8978 × 61 gene expression matrix. For every column we set the gene expressions that are not in the top 90 percentile to 0 to filter out noise and focus only on a clear signal with highly expressed genes. These data were related to the individual cluster gene sets using Spearman rank correlation and then normalized across cell types (z-scored) to identify cell types with the highest representation in each cluster. A cell type was classified as enriched with a critical z-score of Z>1.28.

Genetic annotations

For functional profiling of genes biclustered with brain networks we applied the knowledgebase from Ingenuity Pathway Analysis (IPA) (QIAGEN Inc., https://www.qiagenbioinformatics.com/products/ingenuitypathway-analysis) (Krämer et al., 2014). Each cluster

from biclustering of the full lineage or hominid branch was analyzed separately. We applied Nervous System filter to avoid non-specific functional associations. All results are displayed in the Table S6.

Single gene associations in biclusters were taken from OpenTargets database (https://platform.opentargets.org/) (Carvalho-Silva et al., 2019; Ghoussaini et al., 2021). At least 10 genes were sampled from each bicluster of the full lineage and hominid branch biclusterings (given sufficient bicluster size) and inspected for the presence of genetic associations with behavioral/neuronal/psychiatric symptom domains. Aggregate genetic associations were collapsed for each bicluster and compiled into symptom domain categories, depicted in Figures S11 and S9.

Methodological remarks

Taken together this workflow maps ω data onto spatial brain gene expression and correlates it with FNs (Table S7). Both cumulative correlation and biclustering build upon ω-driven spatial correlations of highly selected genes per branch with FNs. Cumulative correlations focus on functional correlations for each PSC top-selected genes, whereas biclustering relates ranked ω of all branches and FNs simultaneously, thereby building clusters of highly selected genes (bound to any branch) that are highly correlated with FNs. Together, these approaches support one another and reconstruct a congruent ancestral history of the brain's functional evolution.

QUANTIFICATION AND STATISTICAL ANALYSIS

Phylogenetic analysis and ω calculation were performed using IQ-TREE (v1.6.10; (Nguyen et al., 2015)) and ModelFinder (Kalyaanamoorthy et al., 2017). Approximately Unbiased tree toplology tests (AU-test, (Shimodaira, 2002)) were used to identify plausible trees (p-value>0.05). ω values (Yang, 1998; Yang and Nielsen, 1998) were calculated using *codeml* (implemented in PAML v4.9i; Yang, 2007). Our approach for managing unstable or unreliable estimates of ω′s is described in the STAR Methods section (STAR Methods, ω calculation) of this paper.

Computational neuroanatomy (STAR Methods, Computational neuroanatomy) was conducted in R 4.0.3. An R notebook output (html file) can be found in the Supplementary File 'Computational neuroanatomy code'. Task-evoked functional brain activity from the Human Connectome Project (HCP, 11 FNs, Figure S4, Table S12, (Van Essen et al., 2013)) was identified as significant +/− 5 sigmas from the mean as described in Barch et al. (Barch et al., 2013). For generating ω-weighted maps, weighted spatial gene expression was compared to maps with randomly shuffled ω′s (n = 10000) using z-tests. The Benjamini-Hochberg method was applied to adjust the False Discovery Rate of the p-values. Statistical significance for these maps was determined for adjusted p-values<0.1. Spatial gene expression and ω values were mined via biclustering using GABi (Curry, 2014), and descriptive statistics for each bicluster (mean, standard deviation, and quantiles) are presented in Table S5. Permutation tests were performed to verify that biclusters showed significantly higher mean ω and gene-to-network correlations than random sets of similar size (n = 10000) with p-values<0.0001. Correlations between bicluster gene sets and brain cell types (single cell gene expression data) was normalized across cell types (z-scored), and cell type was classified as enriched with a critical z-score of Z>1.28.